2019

AEG-1 KNOCKOUT SENSITIZES HEPATOCELLULAR CARCINOMA (HCC) CELLS TO IONIZING RADIATION

Maheen Khan
Virginia Commonwealth

AEG-1 KNOCKOUT SENSITIZES HEPATOCELLULAR CARCINOMA (HCC) CELLS TO IONIZING RADIATION

A thesis submitted in partial fulfillment of the requirements for the degree of
Master of Science Virginia Commonwealth University, 2019

By

MAHEEN H. KHAN, B.S.
Department of Biology, Virginia Commonwealth University, 2017
Department of Psychology, Virginia Commonwealth University, 2017

ADVISOR: DR. DEVANAND SARKAR, M.B.B.S., Ph.D.
Professor, Department of Human and Molecular Genetics
Harrison Foundation Distinguished Professor in Cancer Research
Blick Scholar
Associate Scientific Director, Cancer Therapeutics
VCU Institute of Molecular Medicine
Associate Director of Education and Training
Massey Cancer Center

Virginia Commonwealth University
Richmond, Virginia
April 2019

AKNOWLEDGMENTS

First and foremost, I would like to thank my advisor, Dr. Devanand Sarkar, for his immense patience and generosity while mentoring me. He has been a hands-on mentor and guided me to develop both the technical and critical thinking skills a scientist needs. Under Dr. Sarkar's supervision, I began to learn how to identify interesting pieces of data and further pursue their meaning. He has inspired me with his hardworking and passionate character and will remain my greatest role model for a scientist.

I would also like to thank the committee members, Dr. Wang and Dr. Kristoffer Valerie, for their helpful suggestions, insights, and questions.

My sincere thanks also goes to the other members of Dr. Sarkar's lab - Rachel Mendoza, Saranya Reghupaty, and Bryan McKiver (former member). Rachel helped to generate the knockout cell lines and also answered my many technical questions during my year in the lab. Sara and Bryan have been immensely helpful in helping me understand the fundamentals of lab work.

Dr. Chunqing Guo and Gene Clark from Dr. Wang's lab also deserve my gratitude for the numerous times they aided me in irradiating my cells. This project would not have been possible without their willingness to help me in my experiments.

I am also grateful to the personnel in the VCU Flow Cytometry Core - Julie Farnsworth and Dr. XinYan Pei - and Microscopy Core - Frances White. Julie and Dr. Pei have been extremely helpful in training me to use the instruments and how to gate my FACS data. Frances was also earnest in helping me to obtain my confocal images.

Finally, I would like to thank my parents, Dr.'s Tahir Khan and Fariha Bangash, and my four younger siblings for their constant support, love, and laughs. My parents instilled in me the values of hard work and perseverance. My greatest satisfaction is in making them proud. I cannot imagine having completed this project without them by my side.

TABLE OF CONTENTS

I	List of figures		i
II	List of abbreviations		ii
III	Abstract		iv
IV	Introduction		
	a.	Hepatocellular carcinoma	1
	b.	Radiation therapy and radioresistance in HCC patients	2
	c.	AEG-1 structure and function	4
	d.	The Mammalian Cell Cycle	6
	e.	The DNA Damage Response	7
	f.	BCCIP structure and function	10
V	Materials and methods		13
VI	Results		21
VII	Figures		32
VIII	Discussion		51
IX	Future directions		61
X	References		65
XI	Vita		72

LIST OF FIGURES

Figure 1: Knockout of AEG-1 reduces cell survival and cell viability in HCC cells 31

Figure 2: AEG-1 knockout slows cell cycle progression in HCC cells 33

Figure 3: Knockout of AEG-1 reduces in vitro wound healing and invasion in HCC cells 34

Figure 4: Knockout of AEG-1 sensitizes HCC cells to low-dose ionizing radiation 36

Figure 5: Low-dose ionizing radiation induces G2/M accumulation in AEG-1 WT cells 37

Figure 6: Negative regulators of the G1/S transition are upregulated in QGY-7703 AEG-1 WT cells 38

Figure 7: p21 and cyclin E are upregulated in HuH7 AEG-1 KO cells 40

Figure 8: Low-dose ionizing radiation induces increased DSB signaling in QGY-7703 AEG-1 KO cells 41

Figure 9: Downstream kinases in the ATM/ATR signaling pathways are upregulated in QGY-7703 cells following low-dose ionizing radiation 43

Figure 10: Protein expression of DDR signaling proteins in HuH7 cells 45

Figure 11: AEG-1 knockout induces increased histone H2AX phosphorylation 47

Figure 12: BCCIP expression in mouse hepatic liver cells and in tissue culture 48

Figure 13: BCCIP expression is upregulated following low-dose ionizing radiation in QGY-7703 cells, but not HuH7 cells 49

LIST OF ABBREVIATIONS

AEG-1	Astrocyte elevated gene-1
ATM	Ataxia-telangiectasia mutated protein
ATR	Ataxia telangiectasia and Rad3 related protein
BCCIP	BRCA2 and CDKN1A interacting protein
BRCA1	Breast cancer type 1 susceptibility protein
BRCA2	Breast cancer type 2 susceptibility protein
CRISPR	Clustered regularly interspaced short palindromic repeats
DNA	Deoxyribonucleic acid
DMEM	Dulbecco's modified eagle medium
DSB	Double-stranded DNA break
FACS	Fluorescence-activated cell sorting
FBS	Fetal bovine serum
Gy	Gray, SI unit for radiation dose
HCC	Hepatocellular carcinoma
HRR	Homologous recombination repair
IF	Immunofluorescence
IHC	Immunohistochemistry
IR	Ionizing radiation
KO	Knockout
MTT	3-(4,5-dimethylthiazol-2-yl)-2,5-diphenyltetrazolium bromide

NHEJ	Non-homologous end-joining
PI	Propidium iodide
RNA	Ribonucleic acid
SSB	Single-stranded DNA break
UT	Untreated

ABSTRACT

AEG-1 KNOCKOUT SENSITIZES HEPATOCELLULAR CARCINOMA (HCC) CELLS TO IONIZING RADIATION

A thesis submitted in partial fulfillment of the requirements for the degree of
Master of Science Virginia Commonwealth University, 2019

By **MAHEEN H. KHAN, B.S**.

ADVISOR: DR. DEVANAND SARKAR, M.B.B.S., Ph.D.
Professor, Department of Human and Molecular Genetics
Harrison Foundation Distinguished Professor in Cancer Research
Virginia Commonwealth University

Liver cancer is the fourth leading cause of cancer-associated deaths globally, and among primary liver cancers, hepatocellular carcinoma (HCC) encompasses 75-85% of all cases. HCC is a highly lethal disease due to limited treatment options – only a small subset of patients qualify for surgical resection or transplantation; the remaining patients often display resistance to radiation therapy or chemotherapy. Overexpression of the oncogene astrocyte elevated gene-1 (AEG-1) is associated with poorer survival and increased tumor recurrence in HCC, and numerous studies show its role in initiation of hepatocarcinogenesis. A prior study also demonstrated AEG-1 expression inhibits senescence by diminishing the ATM/Chk1/Chk2/p53/p21 DNA damage response (DDR) pathway. The aim of this study is to understand if AEG-1 expression promotes radioresistance in HCC. A CRISPR/Cas9 plasmid system was used to delete AEG-1 in the QGY-7703, HuH7 and DihXY cell lines, which model HCC. The cell lines were then treated with ionizing radiation (IR). We find that knockout of AEG-1 in these cell lines induces sensitivity to IR at 2.5 Gy. In response to radiation, AEG-1 wildtype cells more profoundly upregulate ATR, Chk1, and Chk2 signaling; and also more rapidly induce γH2AX, ATM, and BRCA1 signaling, which sense dsDNA breaks to initiate homologous recombination repair. We conclude that

AEG-1 expression protects HCC cells from IR through two mechanisms: 1) rapidly initiating the DNA damage response; and 2) increasing replication fork stabilization. These findings indicate AEG-1 can be a therapeutic target in combination with radiation treatment to improve outcomes for HCC patients who demonstrate radioresistance.

Keywords: Hepatocellular carcinoma, ionizing radiation, astrocyte elevated gene-1, DNA damage response

CHAPTER 1

INTRODUCTION

Hepatocellular carcinoma

Liver cancer has the sixth highest incidence of all cancers globally, and is the fourth leading cause of cancer-associated deaths. Among males, liver cancer is the second highest cause of cancer-related deaths, and has the fifth highest incidence of all cancers. According to the most recent global cancer statistics report, approximately 841,000 new cases of liver cancer and 782,000 liver-cancer-associated deaths are reported world-wide. The incidence of liver cancer is increasing in Western nations due to the growing obesity epidemic in these areas – the incidence of HCC is strongly associated with diabetes. Among primary liver cancers, hepatocellular carcinoma (HCC) encompasses 75-85% of all cases[1].

HCC is often an end-stage liver disease that is secondary to infection by hepatitis B virus (HBV) or hepatitis C virus (HCV), both of which lead to chronic inflammation and liver cirrhosis. 50% of all HCC cases are attributed to chronic HBV infection. On the other hand, the percentage of HCC patients positive for HCV markers varies geographically, with Japan having the highest percentage (80-90%). HCC is more prevalent among males partly due to increased incidence of viral hepatitis and alcohol-induced cirrhosis; and partly due to hormonal differences, such as association between increased testosterone and advanced hepatic cirrhosis, and the protective effect of estrogen against HBV infection[2].

Anti-viral treatment reduces recurrence and mortality in patients with HBV-associated HCC, while interferon therapy decreases mortality in HCV-associated HCC. Localized HCC can be treated with surgical resection, liver transplantation, and radiofrequency ablation. However, these

methods are not effective in tumors of advanced symptomatic stages. Systemic treatment of HCC is difficult due to its resistance to traditional chemotherapies, including to cisplatin, doxorubicin, and 5-fluorouracil. Sorafenib, a multi-kinase inhibitor that targets the serine/threonine kinase RAF, is FDA-approved for systemic treatment of patients with advanced HCC; however, a clinical trial showed survival was only improved from 7.9 to 10.7 months in sorafenib-treated HCC patients. Chemotherapy and radiotherapy are now used as palliative treatment in patients with metastatic HCC due to demonstrated resistance to both forms of treatment[3,4]. The limited treatment options make HCC a highly lethal disease.

HCC initiates from terminally differentiated, rarely-dividing epithelial cells. The most frequent genes mutated in HCC are those encoding the proteins p53, c-myc, cyclin D1, BRCA2, APC, and PTEN, among others. Activation of the mitogen-activated protein kinase (MAPK) and vascular endothelial growth factor (VGEF) pathways are also highly associated with HCC tumorigenesis and development. Because HCC tumors show heterogeneity in their activated oncogenic signaling pathways and in their mutated genes, it is difficult to establish effective treatments for the disease[4].

Radiation therapy and radioresistance in HCC patients

HCC patients who are not candidates for surgical resection of tumors, constituting some 85% of the patient population, have various other options: radiation therapy, radiofrequency ablation, percutaneous ethanol injection, microwave coagulation therapy, and transarterial chemoembolization (TACE). For many years, clinicians were cautious to use radiation therapy due to the risk of inducing radiation-induced liver disease, which can eventually lead to liver failure. The risk of causing radiation-induced damage to nearby, uninvolved organs was also present. Radiation therapy given in low doses (ranging from 8 to 50 Gy) originally played a

larger role in improving symptoms for patients in palliative care by treating lymph node, bone, and brain metastases from primary HCC tumors. However, advances in imaging and delivery of radiation therapy have increased the use of radiation therapy in the last twenty years for both advanced and metastatic HCC patients. Combination of radiation therapy with TACE has been suggested to improve 5-year survival and reduce recurrence rates following treatment[5].

There are a number of methods of radiation delivery for HCC patients with varying overall survival and recurrence rates. A 2012 Swiss study with a cohort of 138 patients assessed the effectiveness of volumetric modulated arc therapy (VMAT) on modest tumor size. They report the mean survival for HCC patients treated at 45, 60, and 66 Gy were 8.6, 13.5, and 25.9 months, respectively, indicating effectiveness of radiation therapy increases in a dose-dependent manner. However, complete response to radiation therapy was achieved in only 11% of the patients, indicating resistance to treatment[6]. Three-dimensional conformal radiotherapy (3DCRT) is another form of radiotherapy that has found promising results. In a French phase II clinical trial, 80% of patients treated with 3DCRT at 66 Gy were reported to have a complete tumor response. Although the data is encouraging, 22% of internal lesions and 41% of external lesions were recurrent after a mean follow-up of 29 months[7]. Furthermore, a metanalysis of clinical trials using either stereotactic body radiotherapy, radiofrequency ablation, and TACE showed that the highest 1-year overall survival for patients was 82%, while 1-year localized control varied anywhere from 65 to 100%[8].

The conflicting results from studies on treating HCC patients with radiation therapy make it evident that investigating the molecular mechanisms leading to radioresistance of HCC tumors is crucial for improving patient overall survival and reducing tumor recurrence. The identification

and subsequent targeting of a biomolecule involved in tumor radioresistance is a promising method of sensitizing HCC tumors to radiation treatment.

AEG-1 structure and function

Astrocyte elevated gene-1 (AEG-1), also known as MTDH or LYRIC, is an oncogene that was initially cloned in primary human fetal astrocytes[9,10]. The AEG-1 locus is present on human chromosome 8q22 and contains 12 exons and 11 introns[11]. AEG-1, which acts as a scaffolding protein, contains 582 amino acids, with a 51-72 amino acid single-pass transmembrane domain, and lacks identifiable functional or DNA-binding domains. However, an LXXLL motif present in its N-terminal domain interacts with transcriptional coactivators and co-repressors, indicating its function as a scaffolding protein[12]. All tissues ubiquitously express AEG-1 mRNA, although skeletal muscle, heart, and endocrine gland tissues have higher basal expression[13]. AEG-1 is expressed at low levels in wildtype hepatocytes, and is localized to the nucleus in these cells[14]. In transformed HCC cells, AEG-1 is localized to the cellular perinuclear space. When stimulated by TNF-α - an activator of the MAP kinase cascade and NF-κB survival pathways - AEG-1 translocates to the nucleus to act as a potential transcriptional co-activator of the CREB-binding protein and NF-κB transcriptional complex[15].

Overexpression of AEG-1 has been indicated in multiple cancer types, including HCC, breast, prostate, non-small cell lung, and colorectal cancers[16]. AEG-1 overexpression in HCC was established by immunostaining using anti-AEG-1 antibody and by microarray of patient HCC liver samples. Primary HCC liver samples show increased AEG-1 staining when compared with normal adjacent liver samples, and HCV-associated HCC tissues show a marked increase of AEG-1 mRNA expression in contrast with normal and cirrhotic liver tissues. HCC-derived cell lines have also been clearly characterized with AEG-1 overexpression. *In vivo* siRNA-mediated

downregulation of AEG-1 significantly suppresses the growth of xenografted HCC-derived tumors[11]. AEG-1 knockout mice lack spontaneous liver tumor formation throughout their lifespan, and treatment of AEG-1 knockout mice with diethylnitrosamine results in high resistance to tumor formation compared to wildtype mice, further establishing AEG-1's role in liver carcinogenesis[17]. Analysis of patient HCC tissue samples corroborate *in vitro* and *in vivo* studies by demonstrating a marked increase of AEG-1 mRNA and protein expression; furthermore, AEG-1 expression levels in patients correlate with the stage and differentiation of HCC[11]. Clearly, AEG-1 can be used as a diagnostic and prognostic marker, and as a potential therapeutic target, in HCC.

AEG-1 promotes cancerous phenotypes through activation of several intracellular signaling pathways. Hepatocytes derived from AEG-1 knockout mice show low activation of NF-κB, indicating that AEG-1 is required for NF-κB activation[17]. *In vitro* upregulation of AEG-1 increases the migration and invasive profiles of HeLa and human glioma cell lines via activation of the NF-κB pathway, while siRNA-mediated downregulation of AEG-1 or of NF-κB decreases these characteristics[15].

The Ras-Raf-MEK-ERK pathway, which regulates cell proliferation and growth in response to extracellular signals such as mitogens, has also been indicated as a target for activation by AEG-1. In AEG-1 overexpression clones, phosphorylated ERK42/44, p38 MAPK, and AKT expression was significantly increased, although there was no change in phosphorylation of the pro-apoptotic kinase JNK. Inhibition of ERK42/44 and p38 MAPK decreased *in vitro* matrigel invasion of AEG-1 overexpression clones, but did not significantly affect proliferation[11]. Akt, ERK1/2, and β-catenin are not regulated by AEG-1 as evidenced by a lack of difference in their phosphorylated forms between AEG-1 KO and wildtype mice[17]. These studies show the role of

AEG-1 overexpression in promoting an aggressive cancerous phenotype by inducing invasive, proliferative, and anchorage-independent growth characteristics, and by inhibiting pro-apoptotic signaling.

Interestingly, AEG-1 has also been implicated in inhibiting senescence and dampening activation of the DNA damage response (DDR) in hepatocytes. In a transgenic mouse model with hepatocyte-specific expression of AEG-1, Srivastava et al. (2012) found that there was an increased number of cells positive for β-galactosidase – a marker for senescence – in cultured wildtype hepatocytes when compared to AEG-1 expressing hepatocytes. Subsequent protein expression analysis of the DNA damage markers ataxia telangiectasia mutated (ATM) protein, ATM and Rad3-related (ATR) protein, Chk1, and Chk2 demonstrated increased phosphorylation of these proteins in the wildtype hepatocytes compared against AEG-1 overexpressing hepatocytes. Therefore, AEG-1 expression may protect transformed hepatocytes from DDR-induced senescence[12]. There have not yet been follow-up studies to elucidate the mechanism through which AEG-1 may directly or indirectly interact with the DDR signaling network. Regardless, it is evident that AEG-1 has diverse roles in initiating hepatocarcinogenesis and protecting transformed hepatic cells from cell death.

The Mammalian Cell Cycle

Eukaryotic cells can be in a dividing or non-dividing state. The non-dividing states include quiescence, senescence, differentiation, and apoptosis. Quiescence is reversible - after receiving mitogenic signals, such as cyclins D and E to de-repress E2F-dependent genes, quiescent cells can re-enter the cell cycle. Differentiated and senescent cells, on the other hand, are permanently withdrawn from the cell cycle. The genes involved in quiescence are a different subset of genes compared to those upregulated during growth or apoptotic inhibition[18].

Cyclin dependent kinases (Cdk's) interact with various protein cyclins to temporally regulate the phases of the cell cycle. The activity of these Cdk's oscillate throughout the cell cycle and each cell cycle phase involves formation of specific Cdk-cyclin complexes. Cdk's regulate cell cycle progression by binding various cyclins, including cyclins A, B, D, and E. Early G1 is regulated by the cyclin D/cdk4 and cyclin D/cdk6 complexes, while S-phase initiation is regulated by cyclins A and E expression[19,20]. The activated cyclin D/Cdk4/6 complex targets retinoblastoma protein, pRb, whose phosphorylation results in progression through G1. Following phosphorylation, pRb releases transcription factors of the E2F family, which activates cyclin E transcription. Cyclin E can then form a complex with Cdk2 to further phosphorylate pRb and promote G1 progression and S-phase entry[21].

Entry into G2/M is regulated by a phosphorylation switch of Cdk/cyclin complexes. Protein phosphatase 2A (PP2A) prevents entry into mitosis by dephosphorylating mitotic Cdk's, and its activity is downregulated in multiple cancer types. Cdc25 activates Cdc2-cyclin B which promotes entry into M phase[22]. Cancer cells with defective G1/S checkpoints may rely on the G2/M checkpoint to avoid apoptosis and continue cell proliferation[23].

G0/G1 and G1/S checkpoints prevent inappropriate DNA replication, while G2/M checkpoint allows for DNA repair. Two families of Cdk inhibitors negatively regulate the cell cycle: the INK family binds cdk4 and cdk6 to inhibit D-type cyclin/cdk complex formation; and p21 which inhibits kinase activity by binding cyclin/Cdk complexes. p21 can therefore inhibit cell cycle progression at the G1/S boundary[24].

The DNA Damage Response

DNA damage may result from a variety of intracellular and extracellular stimuli, and if not resolved, may lead to genomic instability. Ionizing radiation (IR) is one such inducer of DNA

damage. The effects of IR can either be direct (i.e. DNA double-stranded breaks) or indirect (formation of reactive oxygen and reactive nitrogen species). ROS and RNS can induce single-stranded DNA breaks (SSB's) and double-stranded DNA breaks (DSB's), DNA crosslinks, and base damage. Surviving cells after IR will have progeny that are characterized by chromosomal rearrangements, aneuploidy, gene amplification, altered gene expression, and other characteristics of genetic instability[25]. Cells exposed to IR during S-phase are susceptible to replication fork stalling and collapse, base mispairing, and point mutations. On the other hand, IR exposure during mitosis can lead to loss of genetic material and cell death[21].

Genomic instability can predispose a cell to initiating carcinogenesis. Homologous recombination repair (HRR) and non-homologous end joining (NHEJ) are two repair pathways present in mammalian cells that protect genomic integrity in the presence of genotoxic stressors. While NHEJ repairs blunt DNA breaks without sequence homology, HRR restores double-stranded breaks and requires sequence homology in the form of a sister chromatid as a template. HRR can only occur in S and G2 phases due to the availability of CDK1, which is needed for 5'-3' end processing and DNA synthesis recovery. NHEJ, on the other hand, can occur throughout the cell cycle. Although the DNA repair pathways are compartmentalized to facilitate our understanding of their mechanisms, there is likely crosstalk between the pathways. They can complement, counteract, or overlap each other's functions[26].

HRR recruits a multitude of proteins to repair DSB's. Following generation of a DSB, resection of the 5' end creates a 3' single-stranded on each side of the DSB. Replication protein A (RPA) coats the exposed single-stranded DNA (ssDNA), and is then replaced by Rad51 in a Rad54, PALB2, BRCA2-dependent process. Strand invasion from the sister chromatid then occurs to create a Holliday Junction. Cohesin proteins stabilize the strand invasion complex and promote

faithful HRR. DNA replication then ensues using the undamaged chromatid as a template[27]. When HRR is insufficient in cells or if the number of DSB's is too large for the cell to repair, the cells are directed to apoptosis[28].

In response to IR, ATM phosphorylates Mdm2/p53 and Chk2. Stabilization of p53 and its subsequent transactivation of p21 is the slow (2-3 hour) response following IR and results in inhibitory binding of both cyclin D/Cdk4/6 and cyclin E/Cdk2 complexes. Chk2 activation, on the other hand, occurs much faster (<1 hour) and results in inactivation of Cdc25, which also results in inhibitory phosphorylation of the cyclin E/Cdk2 complex[21].

ATR is recruited to stalled replication forks and single-stranded DNA breaks by ATR-interacting protein (ATRIP), which interacts with RPA-bound ssDNA via its acidic checkpoint recruitment domain. The 9-1-1 complex - consisting of RAD9A, RAD9B, HUS1, and RAD1 – along with DNA topoisomerase 2-binding protein (TOPBP1) are recruited to the single-stranded breaks. TOPBP1 phosphorylates and activates ATR, which induces ATR's kinase activity. Subsequently, ATR activates Chk1 via phosphorylation and inactivates CDK1/2 activity[29,30].

Breast cancer type 1 and 2 susceptibility proteins (BRCA1 and BRCA2) function in DSB repair and control mitotic entry in the presence of DNA damage via control of the G2 checkpoint[31]. BRCA1 coordinates MRN and CtIP complex formation, while BRCA2 stabilizes Rad51 filaments[26].

PARP1 is another prominent player in NHEJ, HRR, and base mismatch repair pathways. Briefly, PARP1 senses DSB's and quickly recruits meiotic recombination 11 (MRE11) and Nijmegen breakage syndrome 1 (NBS1) proteins to those sites. Once bound to sites of DNA damage, PARP1 catalyzes the addition of poly(ADP-ribose) chains to itself in addition to DNA repair

enzymes and histones, and then recruits repair factors[29]. There is evidence that when PARP1 is unavailable, single-stranded DNA breaks lead to stalled replication forks, which are then converted to double-stranded breaks to be repaired by HRR[32]. However, elimination of PARP1 does not completely prevent activation of the DDR, suggesting that its role is redundant in these complex pathways[33].

TP53 is a tumor suppressor gene that acts as a central hub for numerous cellular processes, including those controlling apoptosis, growth arrest, cell cycle progression, and DNA repair. The protein product of *TP53*, p53, is coined the "guardian of the genome" due to its ability to induce G1 arrest following DNA damage[34]. It is hypothesized that p53 mutation status determines the survival fate of cells facing large amounts of DNA damage, while cells with smaller amounts of DNA damage are able to appropriately repair DNA damage and begin cycling normally again. Therefore, coordinating multiple signaling pathways is needed to decide whether a cell will increase its DNA repair and survival response, or induce apoptosis, in response to ionizing radiation[35,36].

BCCIP structure and function, and AEG-1 interaction

BRCA2-and-p21-interacting protein (BCCIP) acts as a tumor suppressor gene and has been shown to have a role in the DNA damage response during homologous recombination repair of double-stranded DNA breaks in conjunction with BRCA2. BCCIP also promotes cell cycle arrest at the G1/S checkpoint by enhancing the inhibition of CDK2 activity via binding of CDKN1A/p21. Two isoforms of BCCIP exist in humans, BCCIPα and β, which contain identical N-terminal domains and differ in their C-termini. Both isoforms are localized to the nucleus and are ubiquitously expressed across skeletal muscle, heart, kidney, and brain tissues, among others.

At the G1/S checkpoint and throughout S phase, both BCCIPα and BCCIPβ mRNA expression peak. However, BCCIP's role in interacting with p21 to promote cell cycle arrest is primarily attributed to the α isoform[37].

The clinical significance of BCCIP expression has been investigated in several human cancers, including downregulation of both isoforms in multiple human kidney tumors[38]. In HCC, BCCIP downregulation correlates with reduced survival, increased tumor size, and higher histological grade of tumor in patients. Furthermore, *in vitro* knockdown of BCCIP in human-derived hepatocytes promotes cell proliferation, confirmed by accelerated G1 to S transition in these cells[39]. This suggests an inability of BCCIP to act in the DNA damage response and allow for cell survival despite genetic instability in an HCC model.

In the cell cycle, BCCIP is an upstream regulator of the p53/p21 pathway of G1/S checkpoint inhibition. BCCIPα acts as an upstream regulator of p53 by inducing p53 upregulation, which subsequently increases p21 expression. In a human fibrosarcoma cell line, downregulation of BCCIPα (RNAi-BCCIPα) impairs the G1/S checkpoint. Furthermore, ionizing radiation of the RNAi-BCCIPα cell line with γ-rays at 10 Gy results in hastened progression through G1 and S phases, while cell lines with normal basal expression of BCCIPα are blocked in G1. Downregulation of p21 at the protein and mRNA levels in RNAi-BCCIPα cell line indicates BCCIPα downregulation may lead to a lack of CDK2 inhibition in response to DNA damage[40]. Recently, BCCIP has also been identified as a regulator of mitotic spindle integrity through the C-terminus of BCCIPβ localizing to spindle poles and both of its isoforms interacting with dynein and dynactin; however, this function appears to be independent of its function in the DNA-damage-response[41].

There is strong evidence suggesting BCCIP's role in the HRR pathway. Radiation-induced RAD51 foci colocalize with BCCIP in HRR. BCCIP and BRCA2 foci also co-localize in the nucleus in an ionizing-radiation-independent manner, although there is no increase in BCCIP foci in response to ionizing radiation. RAD51 foci co-localization with BCCIP occurs in a dose-dependent manner of ionizing radiation. This suggests RAD51 foci co-localization, but not BRCA2 foci co-localization, with BCCIP is involved in the DNA damage response in response to ionizing radiation. Subsequent downregulation of BCCIP results in decreased formation of RAD51 and BRCA2 foci[42]. Furthermore, BCCIP suppression increases spontaneous single-stranded and double-stranded DNA breaks in the absence of ionizing radiation[43].

There is some preliminary research on the interaction between AEG-1 and BCCIP. In prostate tumor cells, co-transfection of AEG-1 and BCCIPα in a yeast two-hybrid system demonstrate a decrease in BCCIPα protein levels, and overexpression of AEG-1 induces proteasomal degradation of BCCIPα. Proteasomal-mediated-downregulation of BCCIPα protein levels was shown to depend on presence of the intact NH2-terminal domain of AEG-1, as demonstrated by flag-tagged constructs with sequence deletions of AEG-1[44]. However, it is unknown if BCCIPα directly binds the NH2-terminal domain of AEG-1, or if BCCIPα degradation is a consequence of downstream activity mediated by the amino terminus binding to other signaling molecules.

Due to the role of BCCIPα in the DNA damage response, and due to its interaction with AEG-1, further studies delineating the potential role of AEG-1 in the DNA damage response can help us better understand how HCC cells are able to overpass cell cycle checkpoints and continue replicating their genomes despite exogenous DNA damage. Therefore, this may clue us into a mechanism of radioresistance that occurs in HCC.

CHAPTER 2

MATERIALS AND METHODS

Generation of AEG-1 knockout (KO) cell lines

The DihXY cell line is a diethylnitrosamine-induced HCC mouse hepatic cell line. The cell line was generously provided by Dr. Michael Karin's laboratory.

The QGY-7703 cell line was derived from a 30 year-old female human patient with aggressive HCC. QGY-7703 cells also express AEG-1 at very high levels[11]. The cell line was obtained from Fudan University, Shanghai, China.

The HuH7 cell line is a human-derived, well-differentiated hepatic cell line that was originally obtained from a 57 year-old male with HCC. The cell line was generously provided by Dr. Paul Dent's laboratory.

AEG-1 knockout was attained in each of the above cell lines using the Crispr/Cas9 system. The cloning vector was obtained from GeneCopoeia. The sgRNA targeted *MTDH* at the sequence GACTTCAACAGTCCGCCCATT. The vector contained either puromycin or ampicillin resistance genes with a selective mCherry marker. Cells were pulsed using the Gene Pulser Xcell unit and then seeded at a density of 5×10^6 in 6-well plates. Single clones were isolated and expanded using FACS-sorting for mCherry positive cells. For the DihXY cell line, a single AEG-1 knockout clone (DihXY-A8) was used for subsequent studies. For the QGY-7703 cell line, an AEG-1 knockout clone (QGY-A3), a partial knockout clone (QGY-A7) and a negative clone (QGY-A26) were used for subsequent studies. For the HuH7 cell line, two knockout cell lines (HuH7-A1 and HuH7-A6) and two negative cell lines (HuH7-A5 and HuH7-A12) were

used for initial characterization of the cell lines. The HuH7-A6 and HuH7-A12 cell lines were subsequently selected for radiation studies.

Cell culture conditions

HuH7 and QGY-7703 cell lines were grown in Dulbecco's Modified Eagle Media (DMEM) containing 10% (v/v) fetal bovine serum (FBS), 1% penicillin/streptomycin (PenStrep), and .025% ciprofloxacin. DihXY cell line was grown in DMEM containing 20% FBS, 1% PenStrep, .025% ciprofloxacin; and containing 0.12g phenobarbital, 20μL mouse epidermal growth factor (0.5μg/μL solution), 0.005g hydrocortisone, and 0.5mL insulin per 500mL of media. All cell lines were tested for mycoplasma-free status using a Mycoplasma Detection Kit (Thermo Fisher Scientific). Cell lines were used for a maximum of 10 passages, and maintained at 37°C in a humidified atmosphere containing 5% CO_2.

Radiation treatment

For cells treated with radiation, they were subjected to ionizing radiation at a dose rate of 1-2 Gy/minute. DihXY cells were treated with 2.5, 5.0, and 10.0Gy; while QGY-7703 and HuH7 cells were treated at 2.5 and 10Gy.

Colony formation assay

500 cells were plated in 6cm dishes in triplicates per condition. For cells treated with ionizing radiation or sorafenib, cells were plated at least 6 hours prior to treatment in order to allow cells to adhere. Media was replaced every 4 to 5 days. 13 days after plating, cells were fixed with 10% formaldehyde, gently rinsed with DI water and then incubated with a 25% working Giemsa solution. After 1-hour incubation in stain, cells were rinsed thrice gently with DI water.

MTT assay

2000 cells per well were seeded in 96-well plates and incubated in a 10% (3-(4,5-Dimethylthiazol-2-yl)-2,5-Diphenyltetrazolium Bromide) (MTT) solution for 4 hours at either 24, 48, 72 hours, or at 48, 96, 144 hours post-seeding. Following incubation in MTT, 10% sodium dodecyl sulfate (SDS) solution was added to cells. After incubating cells overnight, absorbance was measured at 600nm using a GloMax microplate reader. For cells that received sorafenib treatment, cells were seeded at the above density and allowed to adhere for 6 hours prior to sorafenib treatment. For irradiated cells, cells were first plated in 6cm dishes and then trypsinized and seeded in the 96-well plate following radiation.

Flow cytometry

To assess cell cycle progression in untreated QGY-7703, HuH7, and DihXYXY cells, cells were synchronized using a double thymidine block to accumulate cells at the G1/S border and subsequently released into S-phase. Thymidine was purchased from Sigma-Aldrich (catalog # T1895). Cells were plated at a density of 2.5 x 10^5 cells in 10cm dishes. 200mM thymidine solution was added to cell culture media to a final concentration of 2mM. Cells were first blocked for 18 hours; then released with fresh DMEM for 9 hours; and blocked a second time for 17 hours. Following release with fresh DMEM from the second block, cells then fixed with cold 70% EtOH, treated with 100µg/mL RNase (purchased from Invitrogen) and stained with 1.0 mg/mL propidium iodide solution (purchased from Sigma Aldrich, catalog #P4864) overnight at 4^{o}C prior to data acquisition.

For DihXY cells treated with radiation, cells were plated at a density of 2.5 x 10^5 in 10cm dishes at least 6 hours prior to treatment. For FACS collection, cells were fixed with cold 70% EtOH,

treated with 100µg/mL RNase and stained with propidium iodide overnight at 4°C prior to data acquisition.

For QGY-7703 and HuH7 treated with radiation, cells were plated at a density of 2.5 x 10^5 cells in 10cm dishes at least 6 hours prior to treatment. The FITC BrdU Flow Kit (purchased from BD Biosciences, catalog #559619) was used to double-stain samples with 7-AAD and BrdU. Following radiation, HuH7 cells were pulsed with 1mM BrdU solution for 30 minutes (BrdU incubation time was optimized in untreated HuH7 cells). Cells were then washed with DPBS and fresh media was added. Cells were fixed and stained with anti-BrdU and 7-AAD per the staining kit protocol. Briefly, cells were trypsinized, treated with Cytofix/Cytoperm Buffer for 20 minutes at room temperature, treated with Cytoperm Permeabilization Buffer Plus for 10 minutes on ice, and treated a second time with Cytofix/Cytoperm Buffer for 5 minutes on ice. Cells were then treated with DNase for 1 hour at 37°C, stained with anti-BrdU for 20 minutes, and then stained with 7-AAD overnight at 4°C prior to data acquisition. Negative controls were cells pulsed with BrdU and either 1) stained with neither anti-BrdU nor 7-AAD; 2) stained with anti-BrdU; or 3) stained with 7-AAD.

For QGY-7703 cells, cells were collected at 30 minutes post-radiation or post-double-thymidine-block and subsequently every 4 hours for 12 hours. For HuH7 cells, cells were collected at 30 minutes and subsequently every 6 hours for 48 hours. For cells, cells were collected at 30 minutes and subsequently every 4 hours for 24 hours.

BD FACSCanto™ II Analyzer and FACSDIVA software at the VCU Flow Cytometry Shared Resource Core was utilized to acquire and analyze data. Flow cytometry data was analyzed using FlowJo data analysis software.

Immunohistochemistry

Immunohistochemistry was used to analyze BCCIP expression in previously obtained Cre*/lox* AEG-1 knockout, and wiltype AEG-1, hepatic tissues of C57BL/6 mice[45]. Briefly, paraffin-embedded tissues were fixed to glass slides and incubated at 60 ^{o}C for one hour. Slides were then incubated in xylene twice to de-paraffin the tissues. 100%, 90%, 80%, and 70% EtOH were used to rehydrate the tissues. Subsequently, tissues were incubated in water and PBS for 5 minutes each. Antigen retrieval buffer was applied to the tissues for 10 minutes in microwave, and then rinsed with PBS. 2% hydrogen peroxide was used to quench endogenous hydrogen peroxidase for 20 minutes, and then rinsed with PBS. Slides were blocked in 5% goat serum for 1 hour at room temperature. Slides were incubated in primary antibodies (AEG-1 and BCCIP) overnight at 4^{o}C. Slides were rinsed with PBST thrice for 5 minutes, and then incubated in biotinylated secondary antibody for 1 hour at room temperature. Following secondary antibody incubation, slides were washed thrice for 5 minutes, and then incubated in ABC reagent for 30 minutes at room temperature. Slides were again rinsed thrice with PBST for 5 minutes. Slides were incubated in DAB substrate for 1-5 minutes, then rinsed in water and incubated in hematoxylin for 20 seconds. After rinsing with water, tissues were dehydrated using gradient EtOH, cleaned with xylene, and slides were mounted with permount.

Immunofluorescence

Cells were seeded at a density of 2.5 x 10^4 cells/mL in Millicell EZ slides (Millipore). For cells treated with ionizing radiation, cells were allowed at least 6 hours to adhere prior to treatment. To fix cells, 4% paraformaldehyde was used and then washed thrice with DPBS. Cells were then permeabilized with 0.1% triton solution and washed thrice with DPBS. A 1% bovine serum

albumin, 10% goat serum in 10x PBS solution was used to block cells for 2 hours at room temperature. Following blocking, cells were treated with primary antibody overnight at 4°C. Cells were washed with DPBS and then incubated with a 1:400 dilution of fluorochrome conjugated secondary antibodies in blocking buffer for 1 hour at room temperature. Cells were then washed with DPBS and mounted with DAPI. Negative controls used in this assay were cells incubated with primary antibody, but no secondary antibody. Antibodies used were BCCIP (ProteinTech #16043-1-AP), γ-H2AX (Cell Signaling #9718) and AEG-1. Images were acquired using a Zeiss LSM confocal microscopy at a magnification of 63x at the VCU Microscopy Core, and quantified using ImageJ.

In vitro wound healing assay

2-well silicone inserts were purchased from Ibidi (catalog #80209) to assess cell migration. 70µL of a 5 x 10^5 cells/mL suspension was added to each side of the well, one insert per well in 12-well plates. Cells were allowed to adhere overnight. The insert was removed, which created a 500µM lesion, and fresh media was added to each well. The resulting lesion was imaged at 0, 24, and 48 hours following removal of the insert. Images were obtained with at 4x and 10x magnification. Lesion sizes at 10x magnification at each time point were quantified using the MetaVi Labs online automated cellular analysis system.

Invasion assay

BioCoat™ Matrigel® Invasion Chambers were purchased from Corning. Serum-free DMEM containing 0% FBS was used to rehydrate the inserts for 2 hours at 37°C and 5% CO_2. 750µL of DMEM containing 10% FBS was added to each well in a 24-well plate. Inserts were placed in each well, and 2.5 x 10^4 cells suspended in 500µL serum-free DMEM were added to each insert.

The cells were incubated for 22 hours at 37ºC and 5% CO_2. Following incubation, DMEM-moistened cotton swabs were used to gently remove non-invasive cells from the inserts. The inserts were then fixed and stained with a Diff-Quik staining kit. Images of the invading cells were taken at 10x magnification. The number of invading cells per field were counted manually.

Western blotting

Cells to be collected for total protein lysate were seeded at a density of 1.0 x 10^6 in a 6cm dish. Cells were then washed with DPBS twice and treated with 1.5% n-dodecyl-D-maltoside (DDM) lysis buffer containing PhosStop Easypack phosphatase inhibitor cocktail tablets (Roche) and cOmplete Mini protease inhibitor cocktail tablets (Roche). After lysis, cells were centrifuged at 15000 RPM for 15 minutes. Supernatant was carefully removed and protein concentration was measured using Bradford assay. 20µg to 40µg of protein lysate was resolved in 8 to 12% SDS-PAGE and then transferred on nitrocellulose membranes. Following transfer, cells were blocked in 5% nonfat milk in TBST solution for 1 hour. For primary antibodies to be incubated in bovine serum albumin, membranes were washed 3 x 5 minutes with TBST prior to adding antibody. All membranes were incubated overnight at 4ºC. Prior to secondary antibody incubation, cells were washed 3 x10 minutes with TBST. Secondary antibodies were applied for 1 hour at room temperature. Membranes were washed again 3 x 10 minutes with TBST. Chemiluminescence detection reagents were applied to membranes and images of the proteins were obtained on autoradiography films. EF1α or GAPDH were used as internal controls. Western blot images were quantified using ImageJ.

List of antibodies used:

- Cyclin D1 Cell Signaling #2978
- BCCIP ProteinTech 16043-1-AP

- p21 Cell Signaling #2947
- Phospho-ATR (Ser428) Cell Signaling #2853
- Phospho-BRCA1 (Ser1524) Cell Signaling #9009
- GAPDH Santa-Cruz sc-166545
- Phospho-Chk2 (Thr68) Cell Signaling #2197
- Phospho-Chk1 (Ser345) Cell Signaling #2348
- Chk1 Cell Signaling #2360
- Chk2 Cell Signaling #2662
- p53 Cell Signaling #2527
- γH2AX (Ser139) Cell Signaling #9718
- Phospho-p53 (Ser15) Cell Signaling #9286
- Phospho-ATM (Ser1981) Cell Signaling #5883
- ATM Cell Signaling #2873
- ATR Cell Signaling #13934
- AEG-1
- EF1α Millipore 05-235
- Cyclin E Santa-Cruz sc-481

Statistical analyses

Significance of results was tested using student paired T-test with two-tailed hypothesis. Statistical significance for all data was considered to be a P value of <0.05.

CHAPTER 3

RESULTS

Knockout of AEG-1 using Crispr-Cas9 reduces cell proliferation in HCC cells

AEG-1 knockout was previously achieved in the DihXY cell line[46], and for this study, was successfully replicated in the QGY-7703 and HuH7 cell lines using the Crispr-Cas9 vector. A single knockout and negative (wildtype AEG-1) clone were selected from the HuH7 and QGY-7703 cell lines, along with a partial knockout clone in the QGY-7703 cell line. A negative clone was not available in the DihXY cell line, so the parental cell line was used for AEG-1 WT characterization. AEG-1 expression was confirmed in the knockout and negative HuH7 and QGY-7703 cell lines using western blotting (Fig. 1A). The AEG-1 WT and KO cell lines were initially characterized for cell survival and cell viability. Significantly fewer colonies formed in the AEG-1 KO cell line compared to the AEG-1 WT and partial KO cell lines in the QGY-7703 cell line (Fig. 1B, *P*-values 0.0425 and 0.0163, respectively). However, there was no significant difference in colony formation in the HuH7 cell lines (Fig. 1E). In the MTT assay, QGY-7703 AEG-1 KO cells showed significantly reduced proliferation compared to AEG-1 WT cells at 24-, 48-, and 72-hour time-points (*P*-values 0.00014, <0.00001, and 0.00024, respectively). When the percent cell viability of QGY-7703 AEG-1 KO cells was normalized against AEG-1 WT cells, the AEG-1 KO cells only proliferated up to 78% that of the AEG-1 WT cell line, and did not show exponential growth (Fig. 1C). On the other hand, the HuH7 AEG-1 KO cell line had increased cell viability at all time-points in the MTT assay (Fig. 1D). When the percent cell viability of HuH7 AEG-1 WT cells were normalized against AEG-1 KO cells, the WT cells showed a sharp increase in proliferation after 3 days of incubation. The WT cells continued to increase until they reached 82.5% cell viability of the KO cells after 8 days of incubation.

Knockout of AEG-1 results in decelerated cell cycle progression

After observing the phenotypic effect of AEG-1 knockout in cell proliferation, we sought to characterize the cell cycle profiles of AEG-1 WT and KO cell lines. Although all cell lines demonstrated marked cell cycle acceleration (Fig. 2A-D), this was more apparent in the QGY-7703 WT cells compared to the DihXY cells or HuH7 cells.

Three independent cell cycle experiments were performed on untreated, QGY-7703 cells that were synchronized into the G1/S boundary using a double thymidine block, and subsequently stained with either PI or 7-AAD. For each experiment, 20,000 cellular events were recorded during FACS data acquisition. Cells were gated into G1/G0, S, and G2/M and a percentage of cells in each phase was calculated. These percentages from each independent experiment were averaged and standard deviation error was calculated to determine the reliability of our methods (Fig. 2A). The figure shows that we were able to consistently synchronize the cells into the G1/S boundary and release into S-phase. Furthermore, our results also show that the QGY-7703 cell lines maintain a routine pattern of accumulating in G0/G1 after 12 hours, with the AEG-1 WT cells proceeding more rapidly than the AEG-1 KO cells. Although the error bars are not tight, we argue that this is because the mean and standard deviation were calculated from three data-points, while each of these data-points contained at least 20,000 cellular events. Therefore, we can reliably use this method of analyzing cell cycle progression for our project.

DihXY AEG-1 WT and KO cells were released into S-phase (42.3% and 51.2%, respectively) following double-thymidine block (Fig. 2B). Both KO (55%) and WT (53.1%) cells are maximally in G2/M after 4 hours and complete a round of replication after 8 hours. After 24 hours, KO (72.4%) and WT (47.5%) cells are maximally in G1/G0 once more, completing a second round of replication. However, at 24 hours, WT cells are entering S- (21.7%) and G2/M

(30.7%) phases, while KO cells remain accumulated in G1/G0 (S-phase cells 14.5%, G2/M cells 13.2%), indicating the WT cells are entering a third round of replication more rapidly than KO cells.

Following release of QGY-7703 cells from a double-thymidine block, AEG-1 WT and KO cells were accumulated in S-phase (69.6% and 69.3%, respectively; Fig. 2C). After 4 hours, WT cells accumulated in G1/G0 (75.4%), while KO cells were still cycling in S (49.5%) and G2/M (39%), indicating WT cells had successfully completed replication. KO cells do not accumulate in G1/G0 (70.3%) until 12 hours post-release, at which time WT cells accumulate in G1/G0 again (81%) and have completed a second cycle of replication.

HuH7 AEG-1 WT and KO cells were released into S-phase (59.4% and 73.2%, respectively) after a double-thymidine block (Fig. 2D). Both KO and WT cells complete their first round of replication after 18 hours (data not shown). After 24 hours, WT cells appear to complete a second cycle of replication, at which point they accumulate in G1/G0 (54.1%). At 12-, 24-, and 36-hours post-release, HuH7 AEG-1 WT cells are accumulated in G1/G0 to a higher percent compared to HuH7 AEG-1 KO cells.

Knockout of AEG-1 reduces migration and invasion in HCC cells

To further characterize the effect of AEG-1 knockout in QGY-7703 cells, the Crispr/Cas9 generated cell lines were assessed for their invasive and migratory capabilities. As previously described, AEG-1 has been well-studied in its role in upregulating various cell invasion and migration pathways, including NfκB, MMP2, and MMP9 signaling. Invasion assay using QGY-7703 cells (Fig. 3A, top) showed a significantly increased number of invading cells per field in both the partial KO and WT AEG-1 cells, compared to the KO cells (*P*-values 0.00600 and

0.00596, respectively). Similarly, HuH7 cells assayed for invasive capacity (Fig. 3A, bottom) showed a significantly reduced number of invading cells in the AEG-1 KO cell line compared to AEG-1 WT cells (*P*-value 0.00068). In the wound healing assay (Fig. 3B, top), QGY-7703 AEG-1 KO cells showed significantly reduced cell migration within 24 hours of creating the lesion (*P*-value 0.03968). However, both cell lines equally migrated after 48 hours. There was no significant difference in the initial lesion size (*P*-value 0.26529).

In the HuH7 cell lines, A6 (AEG-1 KO) cells showed significantly reduced cell migration compared to the A5 and A12 (AEG-1 WT) cells after 48 hours (*P*-values 0.01760 and 0.02136, respectively; Fig. 3B, bottom). The initial lesion size between the A6 and A5/A12 cell lines were not significantly different (*P*-values 0.45298 and 0.89823, respectively).

Knockout of AEG-1 sensitizes HCC cells to low-dose IR

In QGY-7703 and HuH7 cell lines, AEG-1 KO cells were significantly sensitized to radiation treatment at 2.5 Gy (Fig. 4A and 4C, respectively). In QGY-7703 cells, *P*-value was 0.00633; in HuH7 cells, *P*-value was 0.02871. Although DihXY AEG-1 WT cells showed marked resistance to IR at 2.5 Gy, the results were not significant (Fig. 4B, *P*-value 0.05602).

Negative and positive regulators of the G1/S transition are upregulated in AEG-1 WT QGY-7703 cells following low-dose IR

After observing sensitization of AEG-1 knockout cells to ionizing radiation, and the differences in cell cycle progression in the cell lines following IR, we decided to study protein expression of signaling molecules involved in the G1/S transition in both untreated cells and cells treated with low-dose IR (2.5 Gy). In QGY-7703 cells treated with 2.5 Gy, there was a 16.7% decrease from G1/G0 in WT cells between 4 to 8 hours, while only 4.8% decrease in KO cells. At 8 and 12 hours, KO cells are 59.1% and 58.8% in S-phase, respectively; while WT cells are 30.8% and

48% in S-phase, respectively (Fig. 5B). This correlates with a decrease in cyclin D1 expression in WT cells at 8 and 12 hours compared to KO cells after IR (Fig. 6C). p-p53 expression was consistently upregulated in WT cells at all time-points following IR at 2.5 Gy. Similarly, p21 expression was upregulated in IR-treated WT cells at 8 hours. On the other hand, in KO cells treated with IR, p-p53 expression decreased at 30 minutes and 4 hours, while it remained unchanged at 8 and 12 hours. Interestingly, p21 expression was downregulated in IR-treated KO cells at 8 and 12 hours when compared to untreated KO cells (Fig. 6A). Total p53 expression in untreated QGY-7703 cells was greater in the AEG-1 WT cell line than in the KO cell line at 8 and 12 hours (Fig. 6B). This observation correlates with greater p-p53 signaling at 8 and 12 hours. When revisiting the cell cycle data, we observe that the untreated QGY-7703 AEG-1 KO and WT cells are maximally in G2/M at 8 hours, and re-entering G0/G1 at 12 hours post-thymidine release (Fig. 2C), indicating p53 expression is transcriptionally activated when these cells are minimally in S-phase. Unexpectedly, bands for p53 were not visible in either WT or KO cells when irradiated at 2.5Gy.

Cyclin D1 expression was increased in UT AEG-1 WT cells compared to AEG-1 KO cells; however, following IR at 2.5 Gy, AEG-1 KO cells showed increased cyclin D1 expression compared to AEG-1 WT cells (Fig. 6C). In both AEG-1 WT and KO cells, cyclin E expression was consistently upregulated after treatment at 2.5 Gy and 10Gy (Fig. 6C). At 30 minutes post-2.5 Gy, cyclin E expression triples in KO cells, compared to untreated cells at the same time-point; while expression in WT cells increases approximately 1.7-fold. At 4 hours post-2.5 Gy, cyclin E expression doubles in both KO and WT cells when compared to untreated cells at the same time-point; however, at 10Gy, expression in KO cells nearly triples, while in WT cells it only increases by about 2.5-fold. Cyclin E expression is reported to be highest during the G1/S

transition[47]; however, in both IR-treated KO and WT cells, cyclin E expression peaks at 8 and 12 hours, while their cell cycle profiles show they are in majority S- or G2/M phase (Fig. 5B).

Positive regulators of the G1/S transition are upregulated in AEG-1 WT HuH7 cells following IR

In the irradiated HuH7 cells, both KO and WT cells had similar cell cycle profiles initially after radiation (KO = 49.6% and WT = 50.8% in G1/G0; Fig. 5A). At 12 and 24-hours post-2.5 Gy, there was a greater percentage of KO cells in G1/G0 than WT. At 24 hours, 24.9% WT cells were in G2/M, compared to only 18.2% of KO cells. After 12 hours, more WT cells have cycled into S (30.6%) and G2/M (34.8%), compared to KO cells (27.6% in S, 29.3% in G2/M). When analyzing protein expression of cell cycle regulators, we found that HuH7 AEG-1 WT cells showed increased expression of cyclin E initially (30 minutes) after thymidine release (Fig. 7B). Afterwards, cyclin E expression remained consistently higher in untreated KO cells when compared against untreated WT cells. This conflicts with the pattern of cyclin E expression in irradiated QGY-7703 cells (Fig. 6C), which showed increased expression in the untreated WT cells at all time-points except at 8 hours. In the HuH7 cells treated with 2.5Gy, cyclin E was initially upregulated in KO cells , while it was downregulated in the WT cells, when compared against their untreated counterparts. After 12 hours, cyclin E was downregulated in both WT and KO cells, although it was decreased approximately 50% in KO cells and 80% in WT cells. At 24 hours following IR, cyclin E expression remained downregulated in KO cells, while its expression was increased in WT cells, compared to their untreated counterparts (Fig. 7B). This replicates a similar observation of cyclin E upregulation in irradiated QGY-7703 AEG-1 WT cells, although the QGY-7703 cells showed a more profound and consistent pattern of cyclin E upregulation (Fig. 6C).

Similar to QGY-7703 cells, p21 expression peaked in both HuH7 AEG-1 WT and KO cells at the last time-point following thymidine release (Fig. 7A), which correlates with WT cells accumulating in G1/G0 (Fig. 2D), but does not corroborate with our observation that KO cells accumulate in S-phase at that time-point (Fig. 2D). Unlike QGY-7703 cells, HuH7 AEG-1 WT cells did not appear to upregulate p21 expression to a higher degree than KO cells following IR at 2.5Gy (Fig. 7A). In the irradiated HuH7 cells, p21 expression appeared to decrease in AEG-1 KO cells at the 12 and 36 hour time-points, which correlate with a lack of robust G1/G0 accumulation at these time-points (Fig. 5A). On the other hand, irradiated AEG-1 WT cells did not show a change in p21 expression at the 12 hour time-point, but p21 expression was downregulated at 24 and 36 hours post-IR when compared to its untreated counterparts.

AEG-1 KO results in delayed DSB signaling compared to AEG-1 WT cells following low-dose IR

In the QGY-7703 cell lines, protein expression of the phosphorylated forms of the DNA double-stranded break sensors ATR and ATM were more strongly upregulated in AEG-1 WT cells at 30 minutes post-IR at 2.5Gy when compared to irradiated AEG-1 KO cells (Fig. 8A and 8C). This pattern of expression was consistent for p-ATR at all time-points following IR, but p-ATM expression had stronger expression in the AEG-1 KO cells starting at 8 hours post-IR at 2.5Gy. Although quantification of γH2AX expression against internal control showed higher expression in irradiated WT cells than irradiated KO cells at 30 minutes (Fig. 8C), the western blot images and IF imaging stained with the same γH2AX antibody (Fig. 11B-C) demonstrated increased signal in KO cells than in WT cells at this time-points. Notably, p-ATR – which has a stronger role in sensing single-stranded DNA breaks and stalled replication forks (reviewed in Haynes, Murai, and Lee, 2018[47]) – was markedly upregulated in both untreated and IR-treated AEG-1 WT cells at all time-points, with the exception of 8 and 12 hours post-IR at 10 Gy (Fig. 8A, C).

p-ATR expression peaks in both WT and KO cells 4 hours post-IR at 2.5Gy; 8 hours following IR at 2.5Gy, WT cells are accumulated majority in G2/M (37.2%), while KO cells are accumulated in S-phase (59.1%). Prior to this time-point KO and WT cells show similar cell cycle profiles, indicating KO cells are arrested in S-phase at 8 hours while WT cells have continued progressing into G2/M (Fig. 5B).

When probing for the downstream checkpoint proteins, p-Chk1 and p-Chk2, in the QGY-7703 cells (Fig. 9) there appeared to be an upregulation of p-Chk2 in both IR-treated cell lines at all time-points, compared to the untreated cell lines. In the WT cells, p-Chk2 expression had more prominent upregulation from 30 minutes to 8 hours post-IR, while expression was increased in KO cells at 12 hours post-IR (Fig. 9A, right, and Fig. 9B, right). There did not appear to be a significant difference in p-Chk1 expression between the two IR-treated cell lines at 30 minutes and 4 hours, however, at 8 and 12 hours post-IR, there was increased signaling in KO cells compared to WT cells (Fig. 9A, left, and Fig. 9B, left).

As for HuH7 cells, p-ATM signaling was initially increased in WT AEG-1 cells following IR at 2.5Gy, but at 12 and 24 hours, KO cells demonstrated increased expression compared to WT cells (Fig. 10A), which is similar to what was observed in QGY-7703 AEG-1 KO cells at 8 and 12 hours post-IR. Although p-BRCA1 expression was greater in irradiated WT cells compared to KO cells at 24 hours post-IR, at 36 hours irradiated KO cells had markedly increased signaling compared to WT (Fig. 10C). In fact, p-BRCA1 expression in KO and WT cells appeared to be downregulated at 30 minutes, 12 and 24 hours post-IR when compared to untreated cells, and this downregulation persisted in KO cells until 36 hours, at which point its expression was upregulated compared to untreated cells. Interestingly, p-BRCA1 expression in WT cells never increased in the irradiated cells when compared against untreated cells at all time-points.

Analysis of p-ATR did not show a remarkable difference between the IR-treated WT and KO clones (Fig. 10B) at 30 minutes and 12 hour post-treatment. However, at 24 hours, the WT cells had increased expression in both untreated and irradiated circumstances. At 36 hours, p-ATR was upregulated in KO irradiated cells compared to untreated cells, while it was downregulated in irradiated WT cells at this time-point.

The downstream signaling kinases p-Chk1 and p-Chk2 in HuH7 cells did not show a similar pattern of expression as in the QGY-7703 cells. p-Chk1 expression (Fig. 10E) was increased in irradiated WT cells compared to KO cells at all time-points, although p-Chk1 in the untreated WT cells was also higher than untreated KO cells at 12, 24, and 36 hours post-thymidine release. p-Chk2 expression (Fig. 10D) on the other hand was greater in irradiated KO cells than WT cells at 30 minutes, 12 hours, and 36 hours. However, compared to untreated cells, p-Chk2 expression was upregulated at 30 minutes and 24 hours in irradiated WT and KO clones, which we did not observe in p-Chk1 expression.

BCCIP is upregulated in AEG-1 KO mice liver tissue, but not in an in vitro *system*

Due to evidence indicating BCCIP downregulation induced by AEG-1 overexpression in prostate tumor cells (Ash et al. 2008), we sought to replicate this observation in HCC cells. Although immunohistochemistry staining of BCCIP in mouse hepatic tissues showed upregulation of BCCIP in the AEG-1 KO samples (Fig. 12A), we were unable to replicate similar results in immunofluorescence staining of DihXY or QGY-7703 AEG-1 KO cells (Fig. 12C). Western blot analysis for BCCIP showed a band approximately 45 kDa that appeared to be downregulated in the DihXY AEG-1 WT clone; however, this band was not observed in the mouse hepatic samples (Fig. 12B). Bands closer to the theoretical size of BCCIP, approximately 36 kDa, were downregulated in two of the mouse hepatic samples, but were unchanged in the DihXY samples.

In HuH7 cells released from a double thymidine block, there did not appear to be a marked difference in BCCIP expression between the untreated cell lines, although expression was increased in KO cells compared to WT cells to some extent at 30 minutes, 12 hours, and 36 hours following release (Fig. 13B).

BCCIP is upregulated in HCC cells following low-dose IR

Because BCCIP is involved in the HRR pathway, we reasoned that inducing DSB's via IR could clue us in to why we were not observing an upregulation of BCCIP in the AEG-1 KO cells. We hypothesized that BCCIP upregulation in AEG-1 WT cells could be an underlying factor in their resistance to radiation treatment. Protein expression of BCCIP in QGY-7703 cells (Fig. 13A) corroborated our hypothesis that AEG-1 WT HCC cells upregulate BCCIP and are resistant to IR. Untreated WT cells and cells treated with 2.5 Gy demonstrated higher expression of BCCIP than KO cells at 0, 4, and 8 hours post-thymidine-release or post-IR; furthermore, BCCIP was not upregulated in KO cells at 8 hours post-IR. However, in UT KO cells was BCCIP expression was higher than that of WT cells. Interestingly, immunofluorescence of BCCIP (Fig. 13C) was steadily increased in AEG-1 KO cells at all time-points following IR at 2.5 Gy. The expression profile of BCCIP in QGY-7703 WT and KO cells is therefore parallel to p-p53 and p21 expression in response to low-dose IR.

Although BCCIP upregulation in response to IR was confirmed through both IF and western blot analysis in the QGY-7703 cell lines, this was not observed in the HuH7 cell lines. Protein expression of BCCIP in HuH7 AEG-1 KO cells was downregulated to a greater extent than WT cells at 30 minutes and 24 hours post-treatment with 2.5Gy IR (Fig. 13B). Interestingly, BCCIP expression was increased in AEG-1 KO cells at 12 and 36 hours post-IR when compared against IR-treated WT cells. These results conflict with both the observation of BCCIP upregulation in

IR-treated compared to untreated cells,, and BCCIP upregulation in WT compared to KO cells, in the QGY-7703 cell lines.

AEG-1 expression in HCC cells is upregulated following ionizing radiation

An unexpected result we observed in the radiation studies was increased AEG-1 signaling in QGY-7703 cells treated at 2.5Gy, as indicated by both western blotting (Fig. 8D, Fig. 13A) and immunofluorescence (Fig. 13C). This increase in signaling was observed by western blotting at 30 minutes until 8 hours post-treatment, but not at 12 hours (data not shown). Meanwhile, AEG-1 signaling was markedly increased in the IF images at 30 minutes post-treatment. However, this increase in AEG-1 signaling was not observed in the HuH7 AEG-1 WT cells (Fig. 10F).

CHAPTER 4

FIGURES

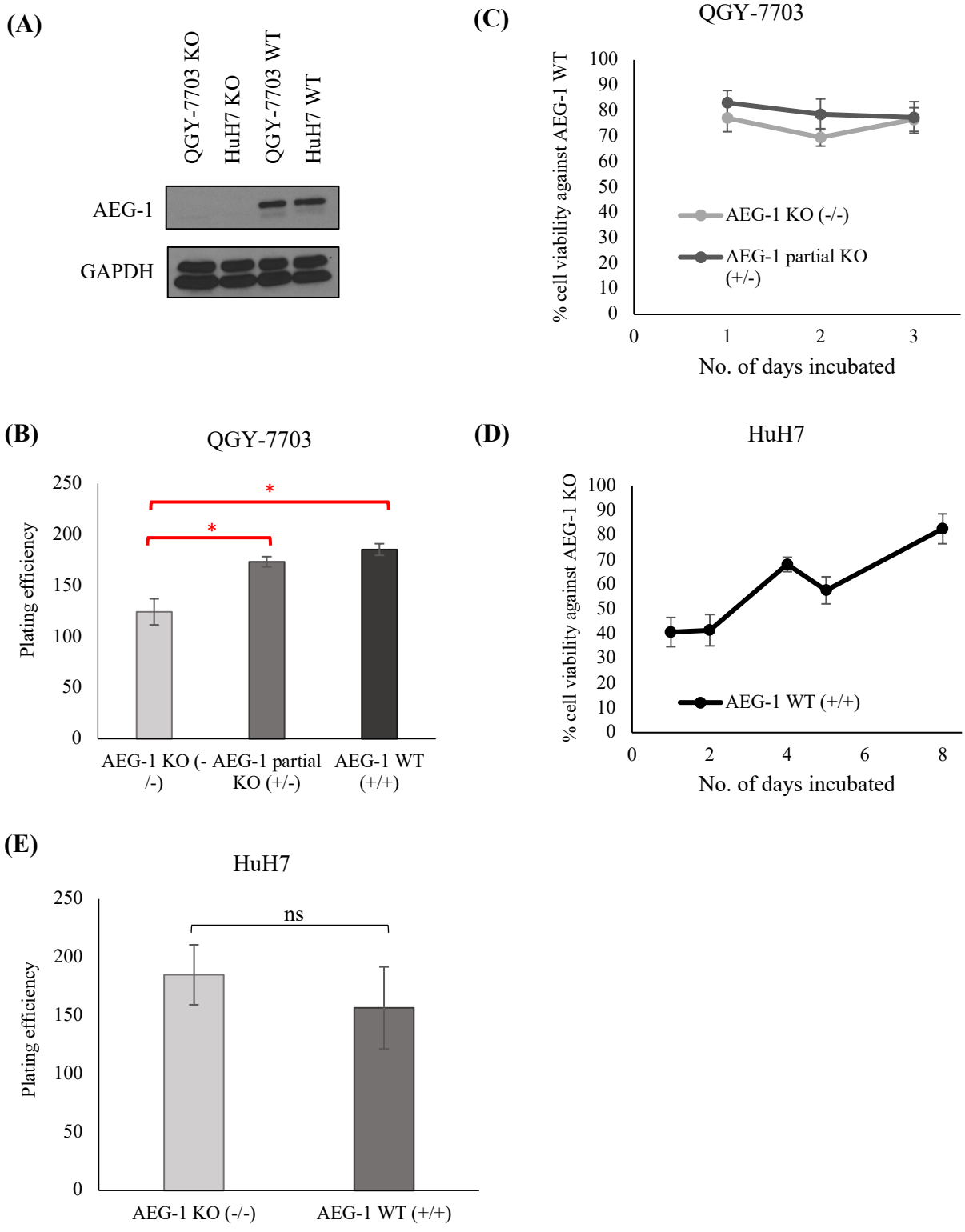

Figure 1 Knockout of AEG-1 reduces cell survival and viability in control, untreated QGY-7703 cells, but not HuH7 cells. (A) Western blot images demonstrate expression status of AEG-1 in the QGY-7703 clones and HuH7 clones. GAPDH was used as an internal control. QGY-7703 cells were assessed for cell survival in (B) colony formation assay and cell viability in (C) MTT assay. Cell viability – measured by the average absorbance at 600nm – of QGY-7703 AEG-1 KO and partial KO cells were normalized against AEG-1 WT cells. (D) Cell viability of HuH7 cells using the MTT assay, shown by the average absorbance of AEG-1 WT cells normalized against AEG-1 KO cells. Although KO cells had increased proliferation at all time-points, WT cells showed a sharp increase in cell proliferation after two days of incubation. (E) Colony formation of HuH7 cells showed there was no significant difference in cell survival between the AEG-1 WT and KO cell lines. * $P<0.05$.

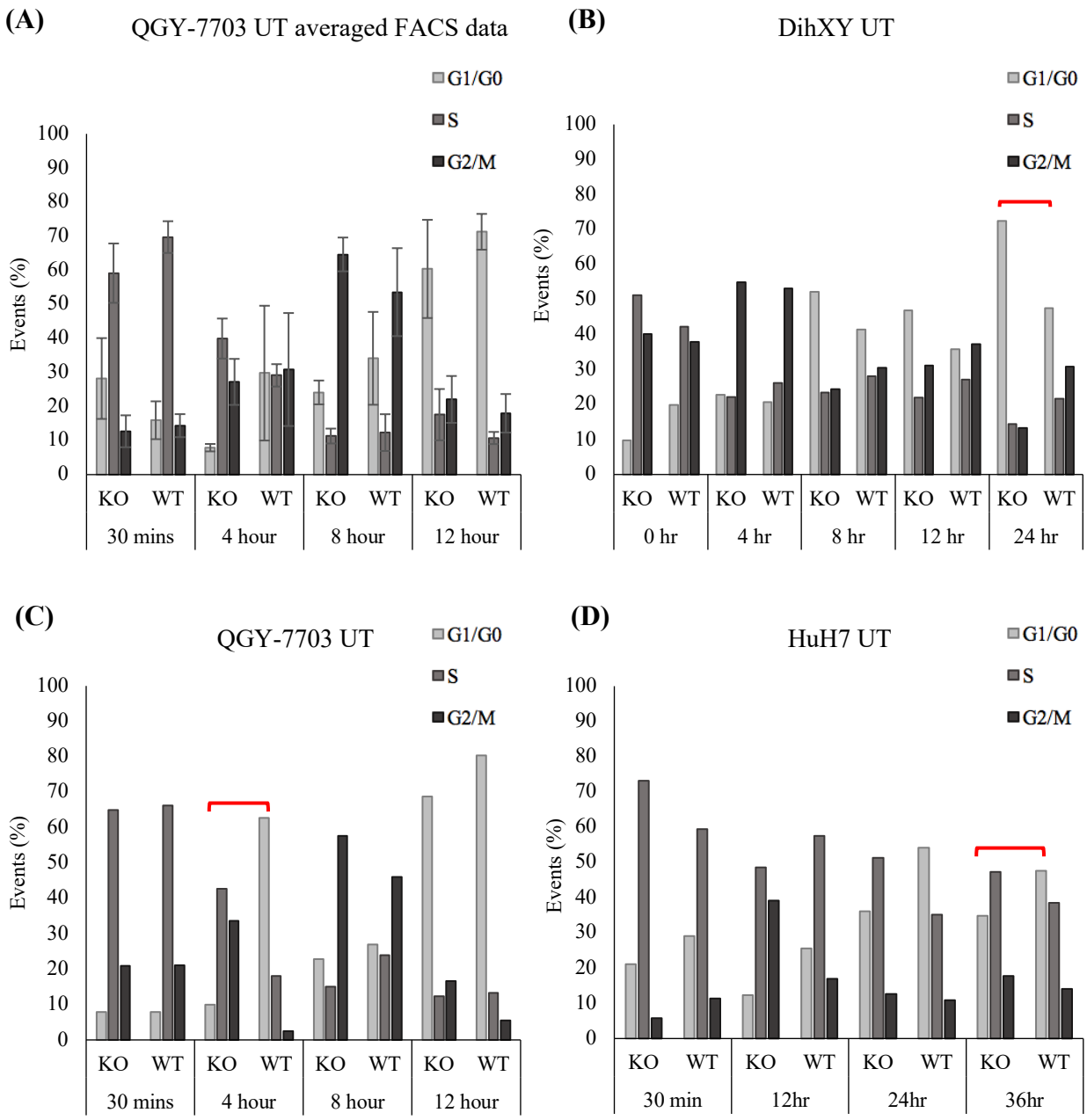

Figure 2 AEG-1 knockout slows cell cycle progression in HCC cells. Cells were treated with a double thymidine block, released into S-phase, and then collected for FACS cell cycle analysis at various time-points. Graphs display the percentage of cells in the total population (>10,000 events per sample) that were in G1/G0, S, or G2/M based on nuclear staining profile. (A) Averaged cell cycle data of three independent experiments using QGY-7703 cells stained with either PI or 7-AAD. (B) DihXY cells stained with PI. After 24 hours, KO cells are maximally in G1/G0 while WT cells are continuing progression into S and G2/M. (C) QGY-7703 cells stained with 7-AAD. 4 hours after release, AEG-1 WT cells have returned to G1, while AEG-1 KO cells are still cycling through G2/M. AEG-1 WT cells completes two cycles after 12 hours, while AEG-1 KO completes 1 cycle. (D) HuH7 cells stained with PI. At all time-points, there are increased AEG-1 WT cells accumulated in G1/G0 compared to AEG-1 KO cells.

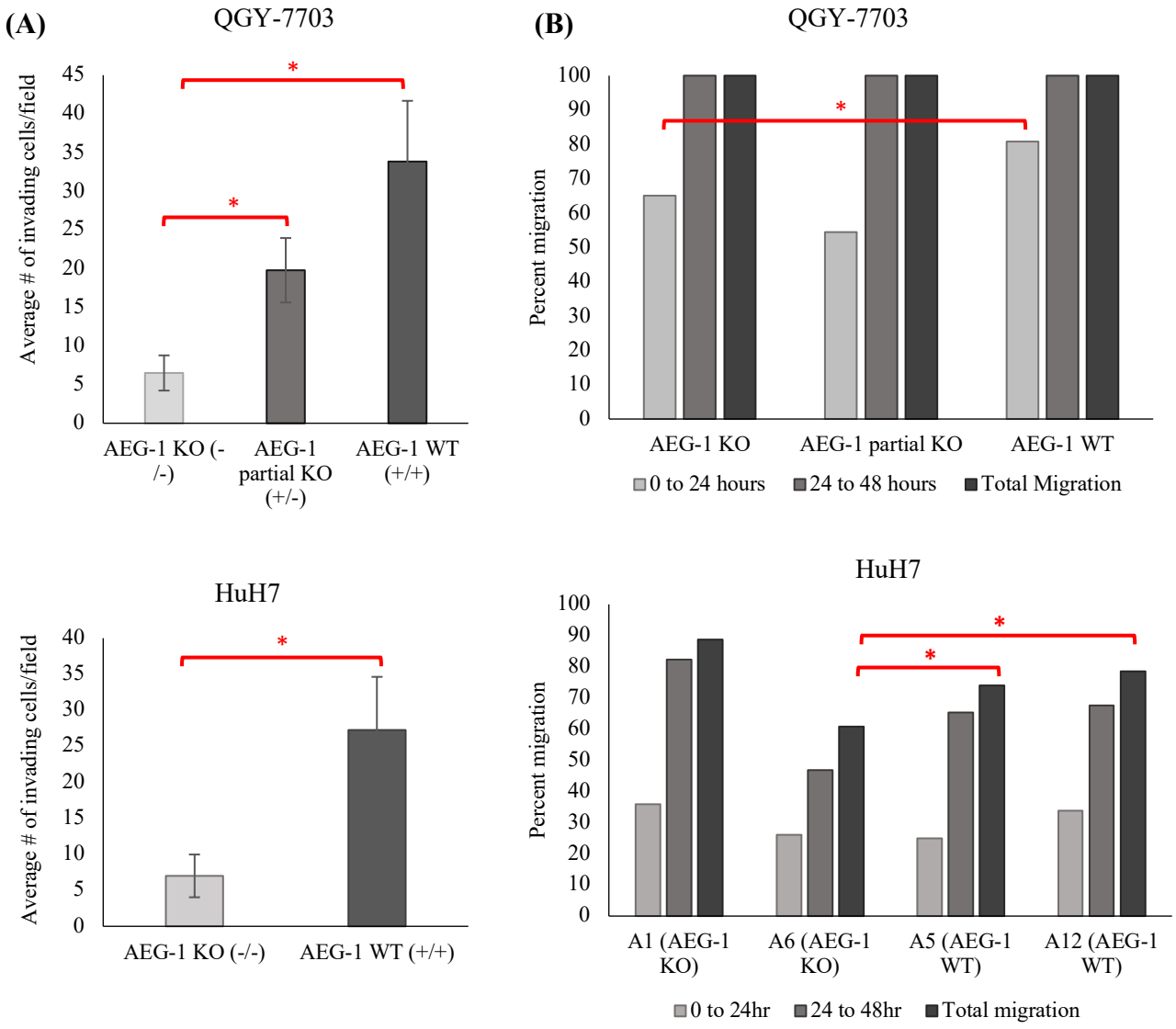
(A)
QGY-7703
Average # of invading cells/field
45
40
35
30
25
20
15
10
5
0
*
*
AEG-1 KO (-/-)
AEG-1 partial KO (+/-)
AEG-1 WT (+/+)
(B)
QGY-7703
Percent migration
100
90
80
70
60
50
40
30
20
10
0
*
AEG-1 KO
AEG-1 partial KO
AEG-1 WT
0 to 24 hours
24 to 48 hours
Total Migration
HuH7
Average # of invading cells/field
40
35
30
25
20
15
10
5
0
*
AEG-1 KO (-/-)
AEG-1 WT (+/+)
HuH7
Percent migration
100
90
80
70
60
50
40
30
20
10
0
*
*
A1 (AEG-1 KO)
A6 (AEG-1 KO)
A5 (AEG-1 WT)
A12 (AEG-1 WT)
0 to 24hr
24 to 48hr
Total migration
(C)
AEG-1 KO (-/-)
AEG-1 partial KO (+/-)
AEG-1 WT (+/+)
(D)
0hr
24hr
48hr

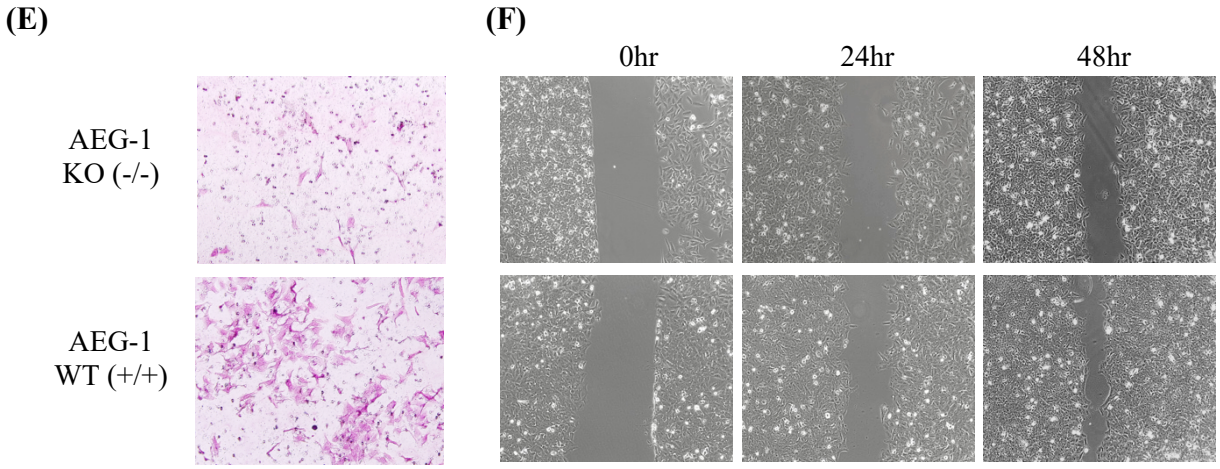

Figure 3 Knockout of AEG-1 reduces *in vitro* wound healing and invasion in QGY-7703 and HuH7 cells. Matrigel invasion assay and wound healing assays were used to assess invasive and migratory capacities, respectively, of QGY-7703 and HuH7 cell lines. (A) AEG-1 WT and partial KO cells showed significantly increased invading cells per field compared to AEG-1 KO cells in the QGY-7703 cell line (top). Similarly, AEG-1 KO in HuH7 cells significantly reduced the average number of invading cells (bottom). (B) AEG-1 KO cells had significantly reduced migration in the first 24 hours compared to AEG-1 WT cells in the QGY-7703 cell line (top). In the HuH7 cell line, the A6 AEG-1 KO cell line had significantly reduced total migration compared to both A5 and A12 AEG-1 WT cell lines (bottom). (C) Representative images of invading cells per field from the QGY-7703 cell line. (D) Representative images of QGY-7703 cell lines in the matrigel invasion assay at 0, 24, and 48 hours following generation of the wound. (E) Representative images of invading cells per field from the HuH7 cell line. (F) Representative images of HuH7 A6 and A12 cell lines in the matrigel invasion assay at 0, 24, and 48 hours following generation of the wound.

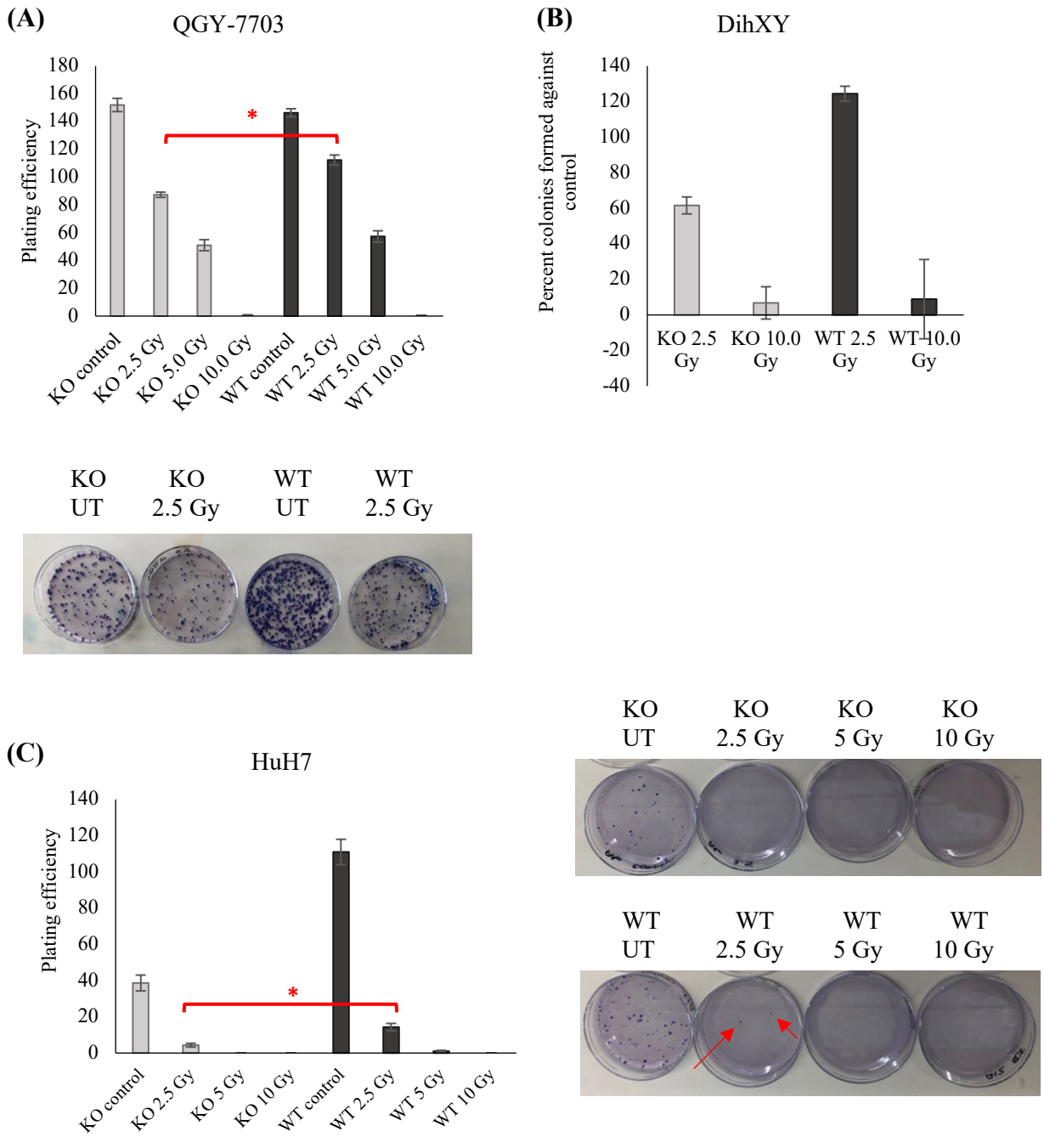

Figure 4 Knockout of AEG-1 sensitizes HCC cells to low-dose radiation treatment. Colony formation assay was used to assess cell survival following ionizing radiation at various doses. QGY-7703 cells (A) and DihXY cells (B) showed significantly reduced survival in the KO cell line at 2.5 Gy. DihXY colony formation is shown as percent colony formation against control. (C) HuH7 cell survival was significantly reduced in the KO cell line following treatment at 2.5 Gy (left). Representative images of colonies in the WT and KO cell lines (right). *P<0.05

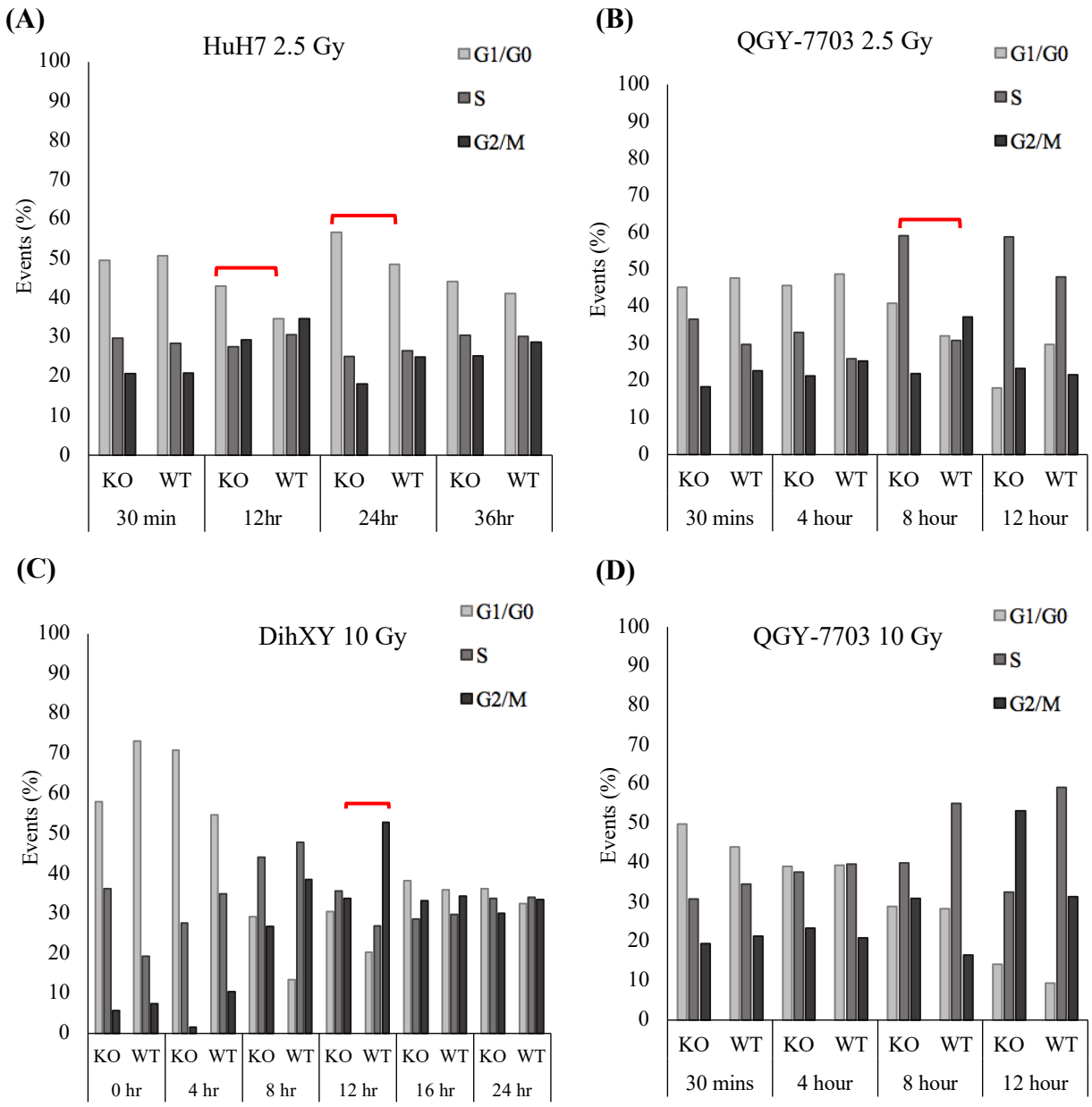

Figure 5 In HCC cells, low-dose ionizing radiation induces greater G2/M accumulation in AEG-1 WT cells, while AEG-1 KO cells at later time-points. Cells were treated with 2.5 Gy [(A) and (B)], or 10 Gy [(C) and (D)] and collected at various time-points. QGY-7703 and HuH7 cells were double-stained with anti-BrdU and 7-AAD. DihXY cells were stained with PI. Graphs display the percentage of cells in the total population (>10,000 events per sample) that were in G1/G0, S, or G2/M based on nuclear staining profile. (A) HuH7 cells treated at 2.5 Gy show increased G2/M accumulation at 12- and 24-hour time-points in the AEG-1 WT cell line, while AEG-1 KO cells accumulate in G1/G0. (B) QGY-7703 cells treated at 2.5 Gy show AEG-1 WT cells are maximally in G2/M at 8 hours, while AEG-1 KO cells accumulate in S-phase at 8- and 12-hour time-points.

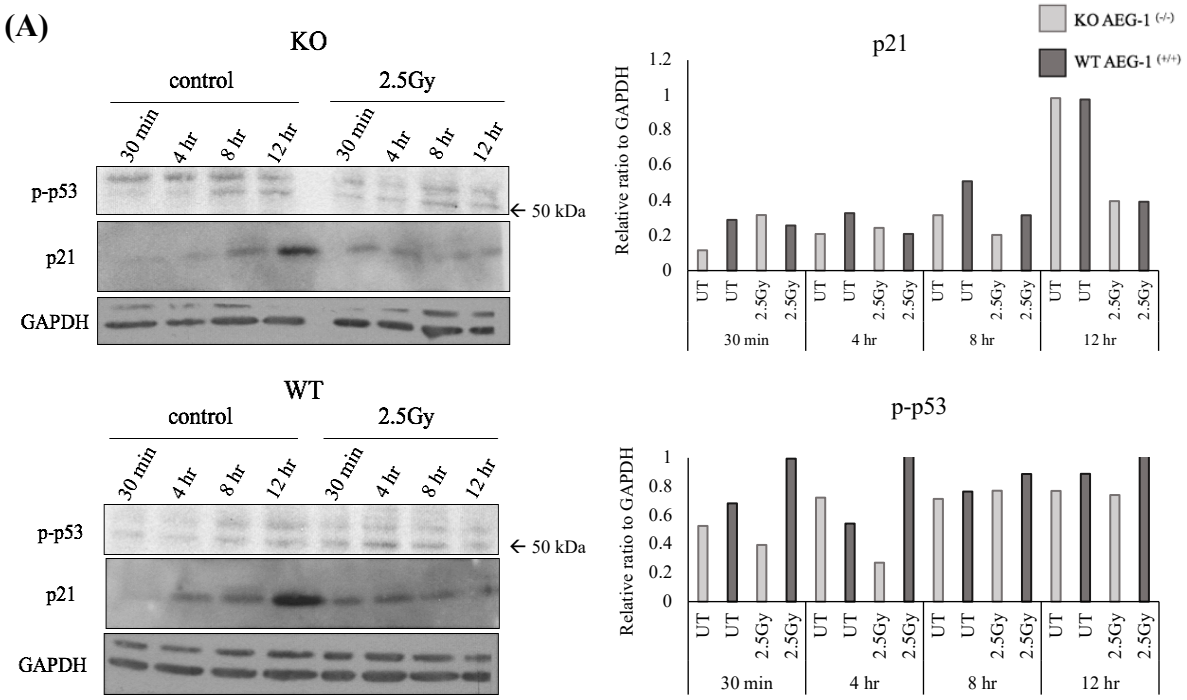
(A)
KO
control
2.5Gy
30 min
4 hr
8 hr
12 hr
p-p53
p21
GAPDH
50 kDa
WT
KO AEG-1 (-/-)
WT AEG-1 (+/+)
p21
Relative ratio to GAPDH
UT
2.5Gy
p-p53

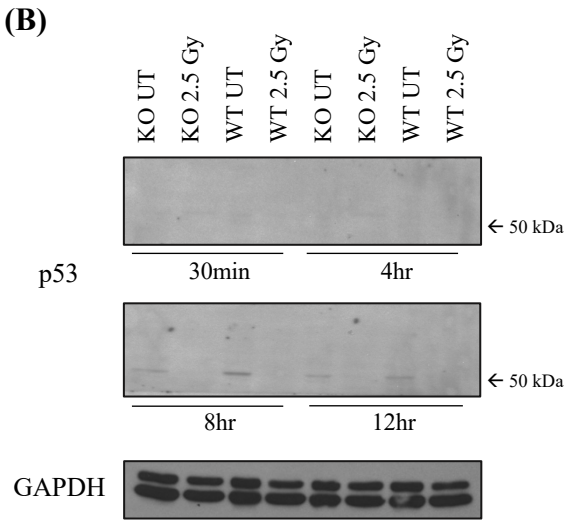
(B)
KO UT
KO 2.5 Gy
WT UT
WT 2.5 Gy
p53
50 kDa
30min
4hr
8hr
12hr
GAPDH

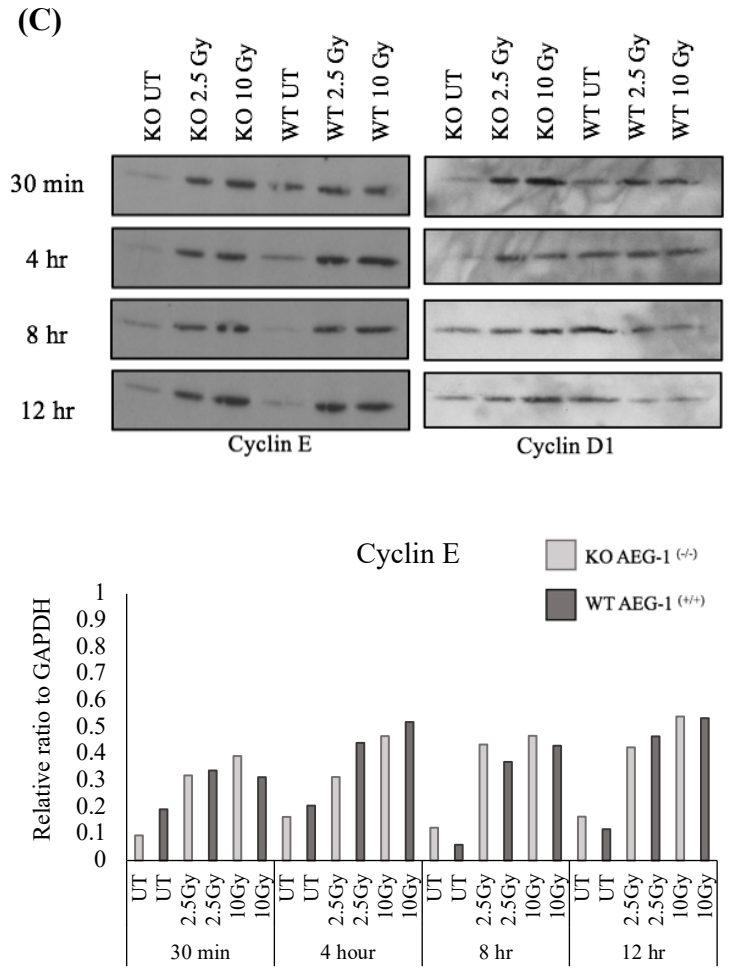

Figure 6 Following low-dose IR of QGY-7703 AEG-1 WT cells, p-p53 and cyclin E protein expression are upregulated, while p21 and cyclin D1 protein expression are downregulated. QGY-7703 cells were collected for whole protein lysate following IR (2.5 and 10Gy) or release from double thymidine block (UT) at 30 minutes, 4 hours, 8 hours, and 12 hours. Lysates were then subjected to SDS-PAGE and probed for negative (A) and positive (C) regulators of the G1/S transition. (A) Western blot images showing expression of p-p53 and p21 in QGY-7703 cells (left) and quantification of expression relative to GAPDH (right). For p-p53, the lower band was used for quantification due to its proximity to the theoretical size of p-p53. P-p53 expression was increased in AEG-1 WT cells following IR at all time-points, while it was downregulated in AEG-1 KO cells at 30 minutes and 4 hours after IR. Meanwhile, p21 expression was downregulated in AEG-1 WT cells at all time-points following IR. In AEG-1 KO cells, p21 expression was initially upregulated following IR, but after 8 hours its expression was downregulated. (B) Western blot images showing total p53 expression in QGY-7703 cell lines. GAPDH was used as an internal control. (C) Western blot images showing expression of Cyclins E and D1 (left) and quantification of expression of cyclin E relative to GAPDH (right). Cyclin E expression was upregulated in both KO and WT AEG-1 cells following both doses of IR.

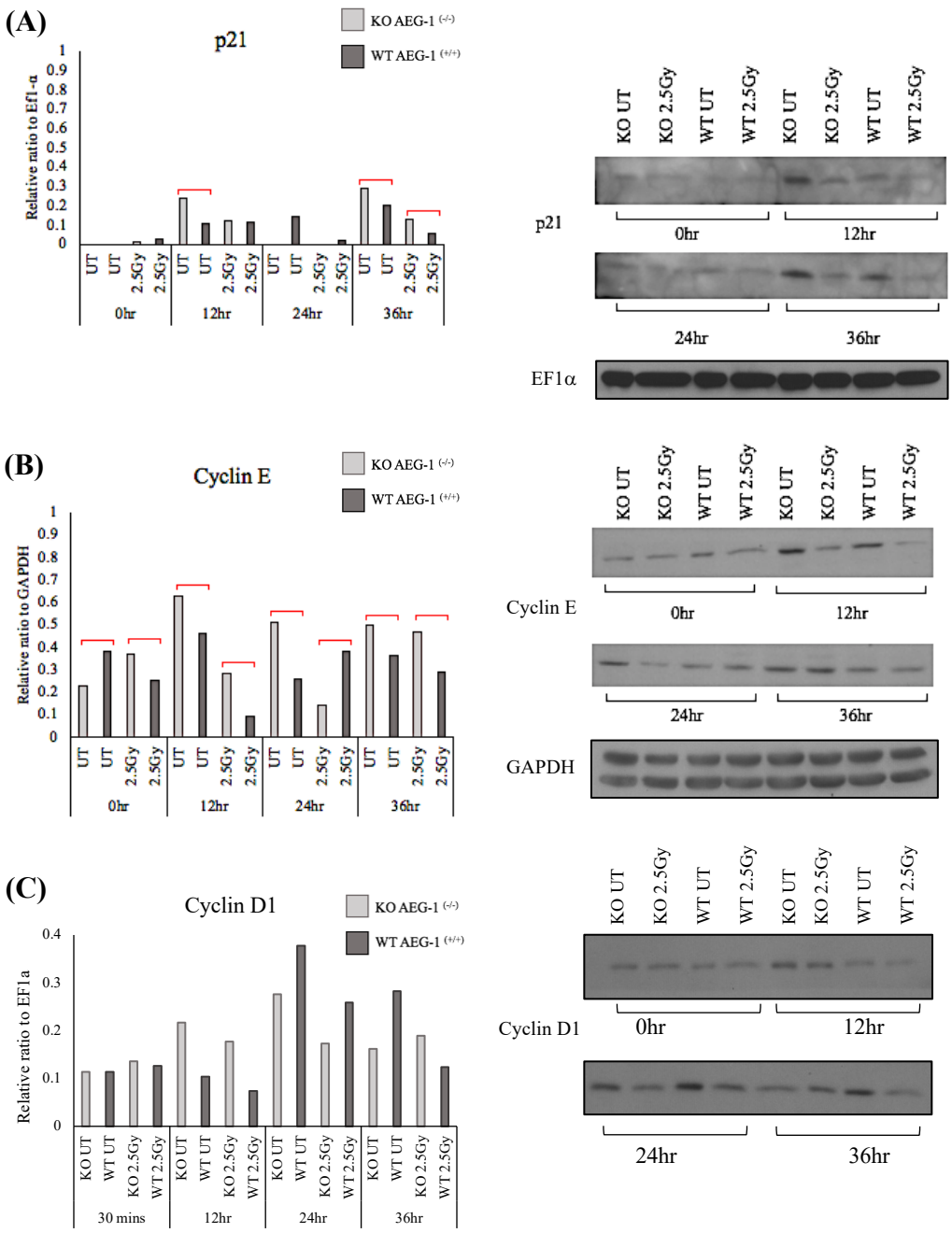

Figure 7 After low-dose irradiation of HuH7 cells, cyclin E protein expression oscillates in both AEG-1 WT and KO cells, while p21 and cyclin D1 expression is consistently downregulated in both WT and KO cells. HuH7 cells were collected for whole protein lysate following IR (2.5Gy) or release from double thymidine block (UT) at 30 minutes, 12 hours, 24 hours, and 36 hours. Lysates were then subjected to SDS-PAGE and probed for negative (A) and positive (B-C) regulators of the G1/S transition. (A) Western blot images showing expression of p21 (right) and quantification relative to EF1α. (B) Western blot images showing expression of cyclin E (right) and quantification relative to GAPDH (left). (C) Western blot images showing expression of cyclin D (right) and quantification relative to EF1α (left).

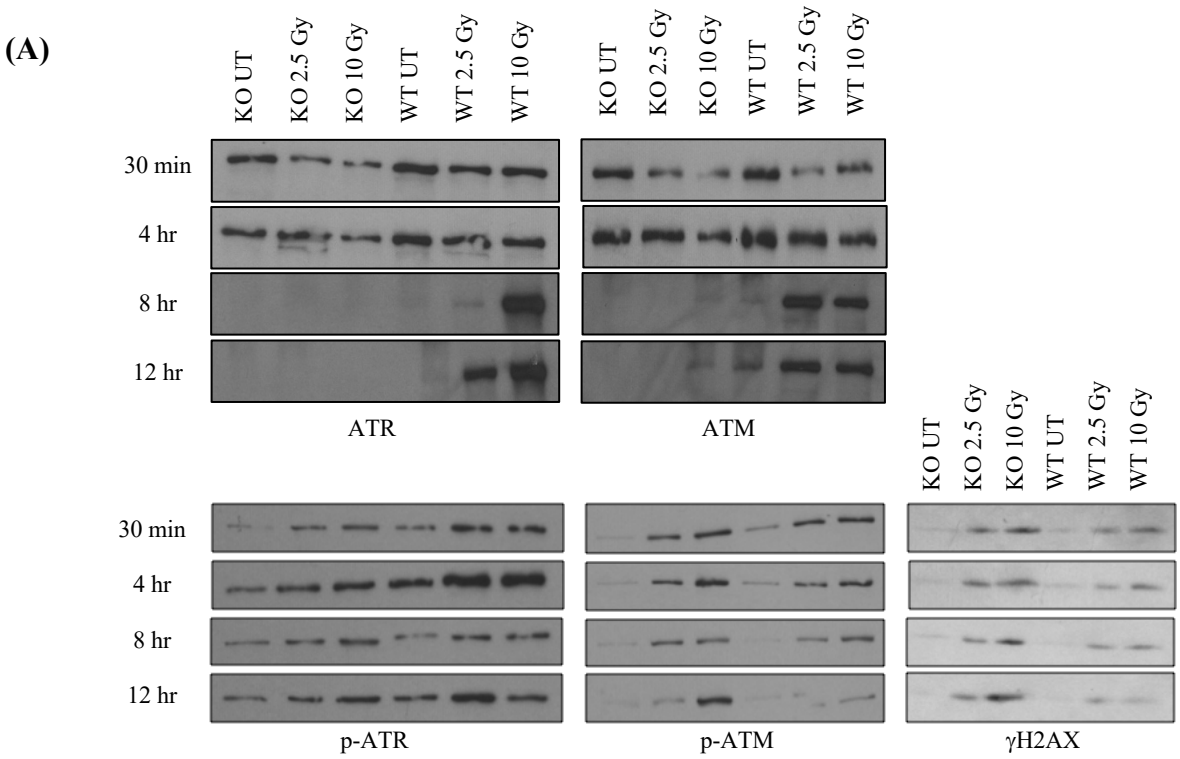
(A)
KO UT
KO 2.5 Gy
KO 10 Gy
WT UT
WT 2.5 Gy
WT 10 Gy
30 min
4 hr
8 hr
12 hr
ATR
ATM
p-ATR
p-ATM
γH2AX

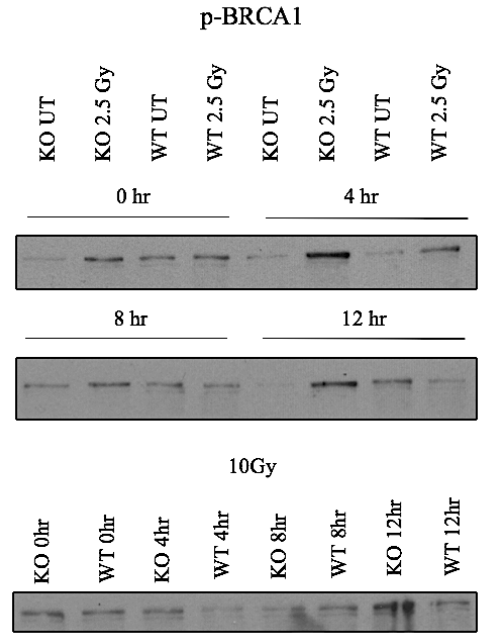
(B)
p-BRCA1
KO UT
KO 2.5 Gy
WT UT
WT 2.5 Gy
0 hr
4 hr
8 hr
12 hr
10Gy
KO 0hr
WT 0hr
KO 4hr
WT 4hr
KO 8hr
WT 8hr
KO 12hr
WT 12hr

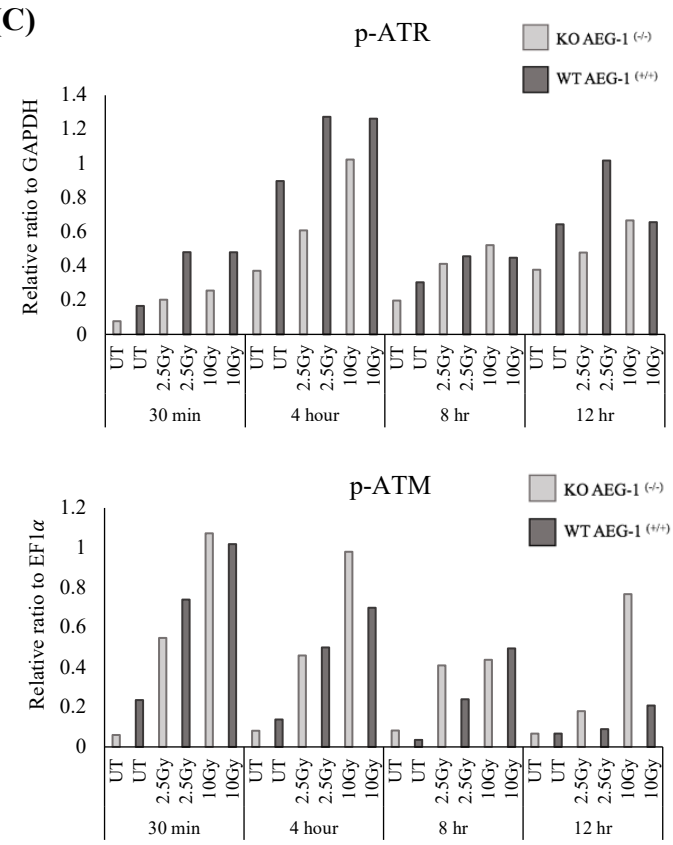
(C)
p-ATR
KO AEG-1 (-/-)
WT AEG-1 (+/+)
Relative ratio to GAPDH
UT
2.5Gy
10Gy
30 min
4 hour
8 hr
12 hr
p-ATM
Relative ratio to EF1α

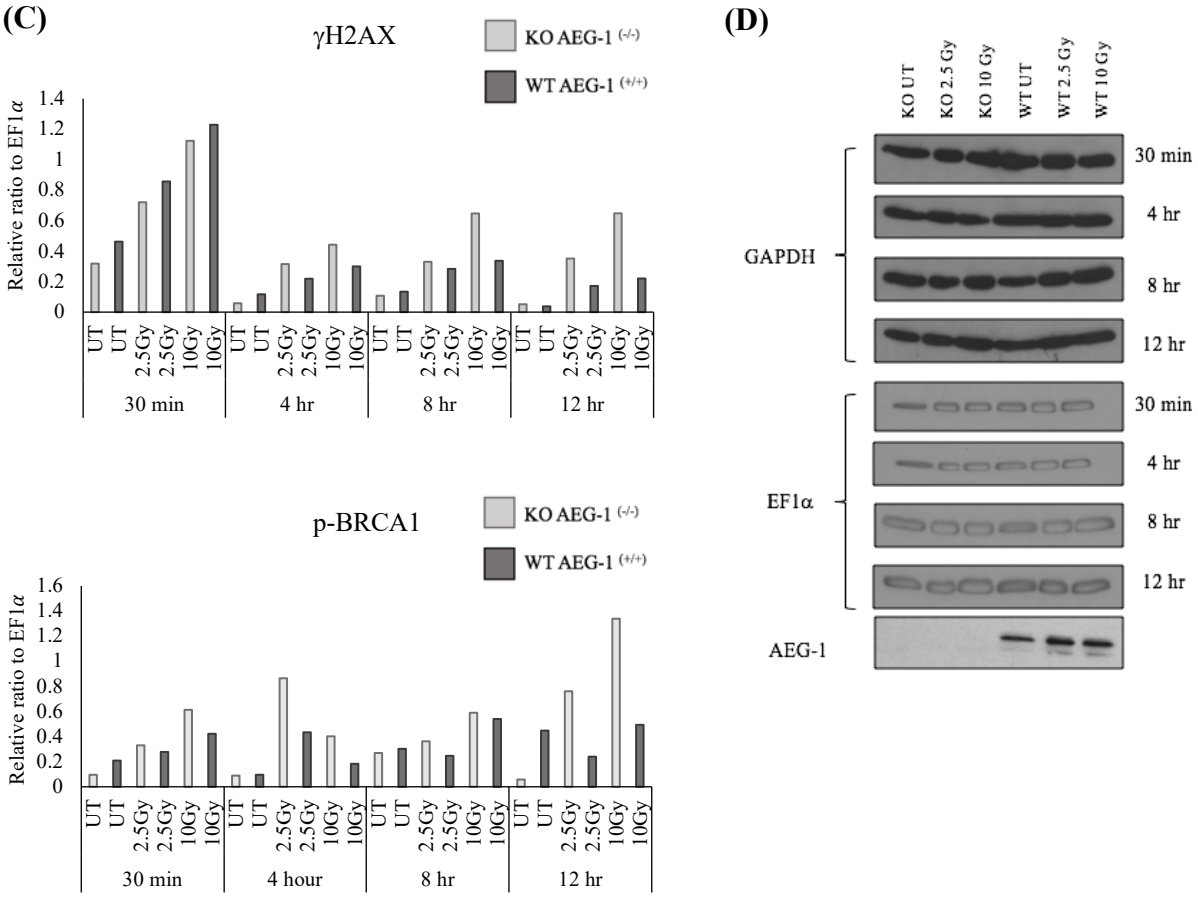

Figure 8 Low-dose ionizing radiation induces strong, rapid DSB signaling in AEG-1 WT cells, while DSB signaling in AEG-1 KO cells begins at later time-points, in the QGY-7703 cell line. QGY-7703 cells were collected for whole protein lysate following ionizing radiation or release from double thymidine block at 30 minutes, 4 hours, 8 hours, and 12 hours. Lysates were then subjected to SDS-PAGE and probed for various DNA damage response markers. (A) Western blots showing total ATR and ATM (top) and p-ATM, p-ATR, and γH2AX expression (bottom). p-ATR and p-ATM signaling were initially greater in AEG-1 WT cells at 30 minutes post-IR at 2.5Gy, while γH2AX signaling was greater in irradiated AEG-1 KO cells at 30 minutes. (B) Western blot showing p-BRCA1 signaling was increased in AEG-1 KO cells following IR at 2.5 and 10 Gy compared to AEG-1 WT cells. (C) Protein expression for p-ATR, p-ATM, p-BRCA1, and γH2AX were quantified using ImageJ against their respective internal controls. (D) Representative blots of internal controls. AEG-1 expression was consistent with KO and WT cell lines.

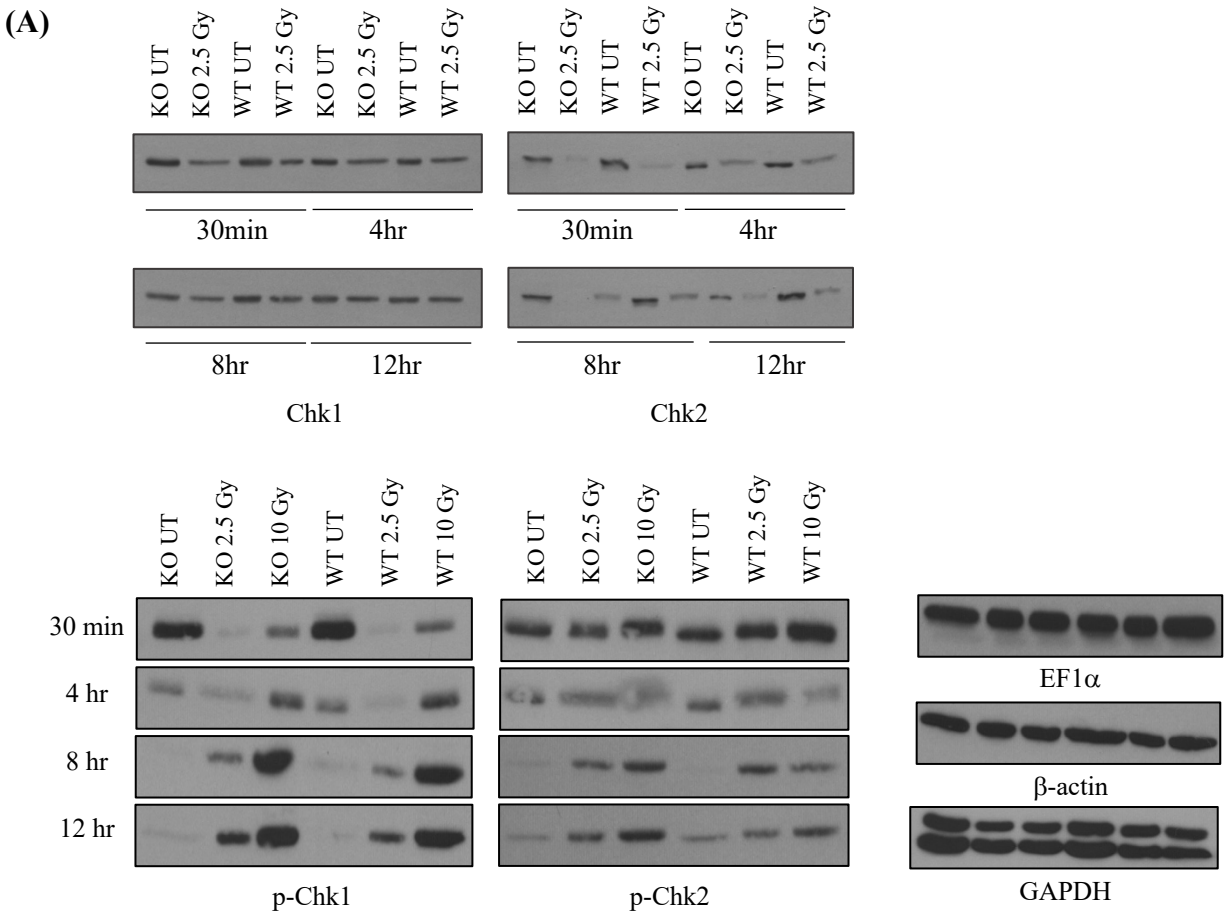
(A)
KO UT
KO 2.5 Gy
WT UT
WT 2.5 Gy
30min
4hr
8hr
12hr
Chk1
Chk2
KO 10 Gy
WT 10 Gy
30 min
4 hr
8 hr
12 hr
p-Chk1
p-Chk2
EF1α
β-actin
GAPDH

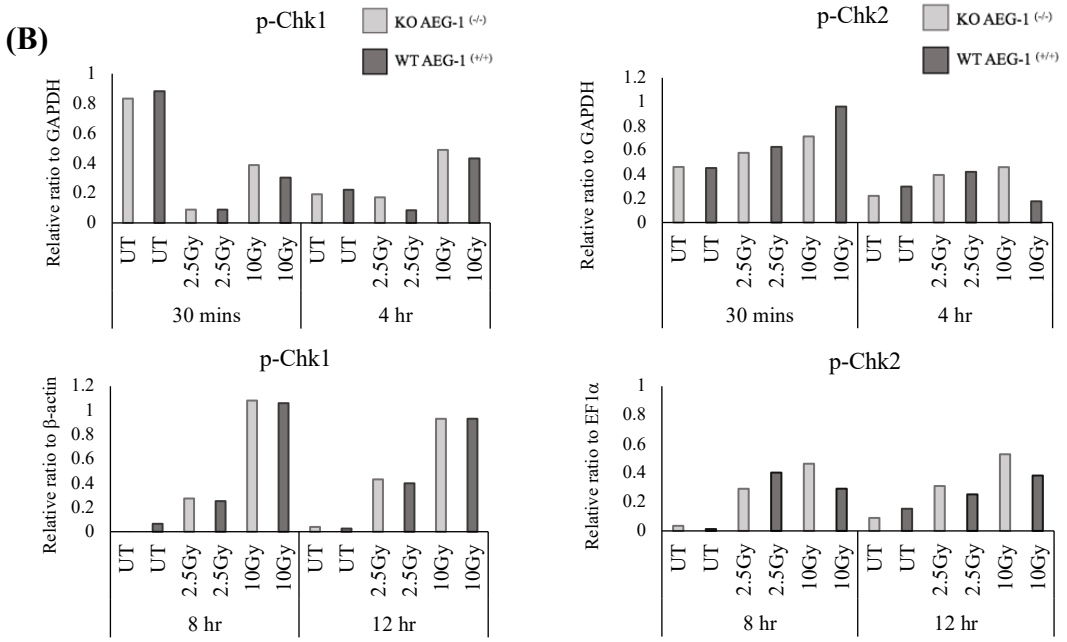
(B)
p-Chk1
KO AEG-1 (-/-)
WT AEG-1 (+/+)
Relative ratio to GAPDH
UT
2.5Gy
10Gy
30 mins
4 hr
p-Chk2
Relative ratio to β-actin
Relative ratio to EF1α
8 hr
12 hr

Figure 9 p-Chk2, but not p-Chk1, is upregulated in QGY-7703 AEG-1 WT and KO cells following low-dose IR. QGY-7703 cells were collected for whole protein lysate following 2.5Gy IR or release from double thymidine block (UT) at 30 minutes, 4 hours, 8 hours, and 12 hours. Lysates were then subjected to SDS-PAGE and probed for p-Chk1 and p-Chk2 expression. (A) Western blot images of p-Chk1 and p-Chk2, and loading controls (far right). (B) Quantification of p-Chk1 (left) and p-Chk2 (right) expression relative to loading controls. p-Chk2 expression was immediately and persistently upregulated in both AEG-1 WT and KO cells after IR at 2.5Gy, while p-Chk1 was upregulated after 8 hours. Both proteins were strongly upregulated after IR at 10Gy.

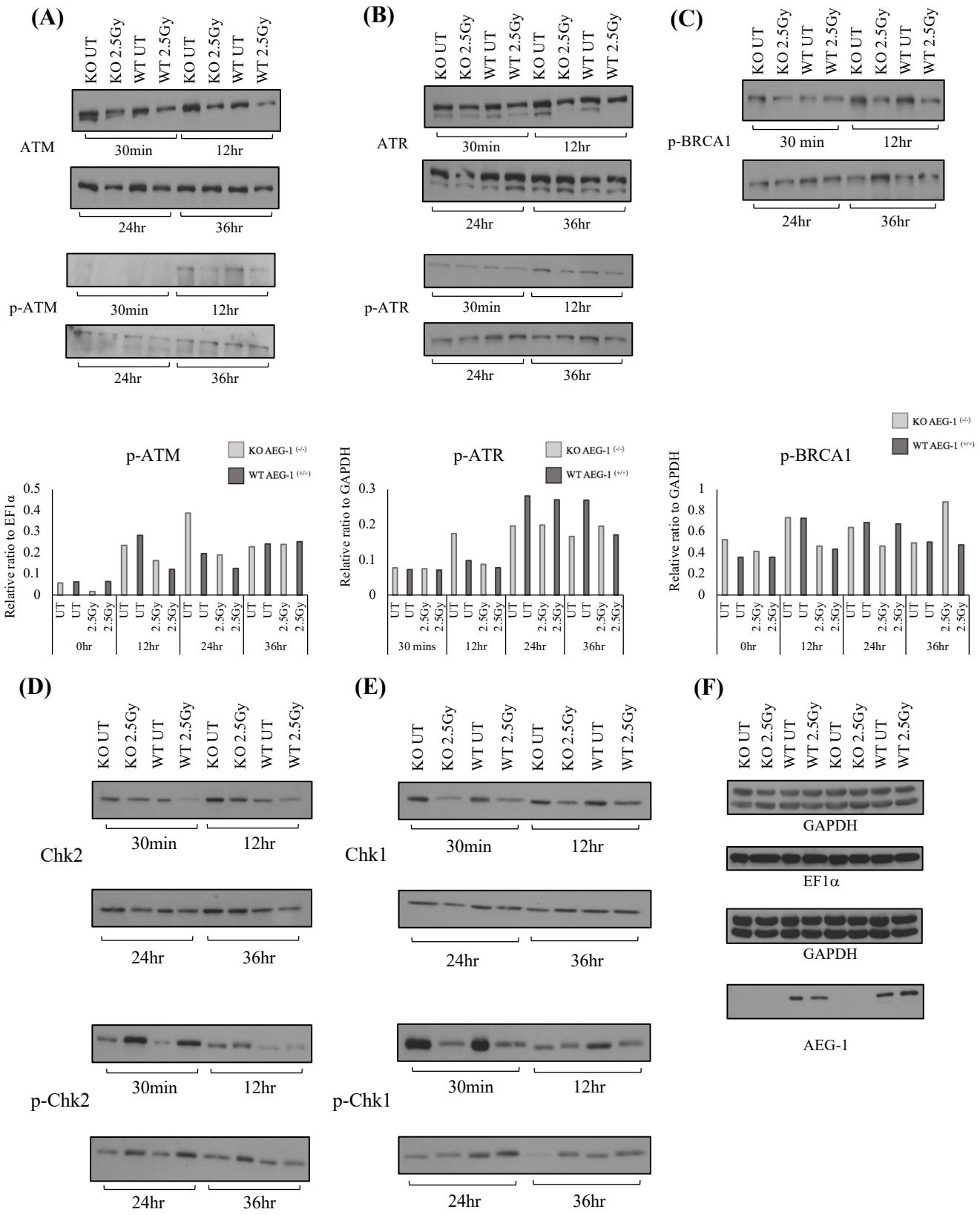
(A)
KO UT
KO 2.5Gy
WT UT
WT 2.5Gy
ATM
30min
12hr
24hr
36hr
p-ATM
(B)
ATR
p-ATR
(C)
p-BRCA1
p-ATM
KO AEG-1 (-/-)
WT AEG-1 (+/+)
Relative ratio to EF1α
p-ATR
Relative ratio to GAPDH
p-BRCA1
UT
2.5Gy
0hr
30 mins
12hr
24hr
36hr
(D)
Chk2
p-Chk2
(E)
Chk1
p-Chk1
(F)
GAPDH
EF1α
AEG-1

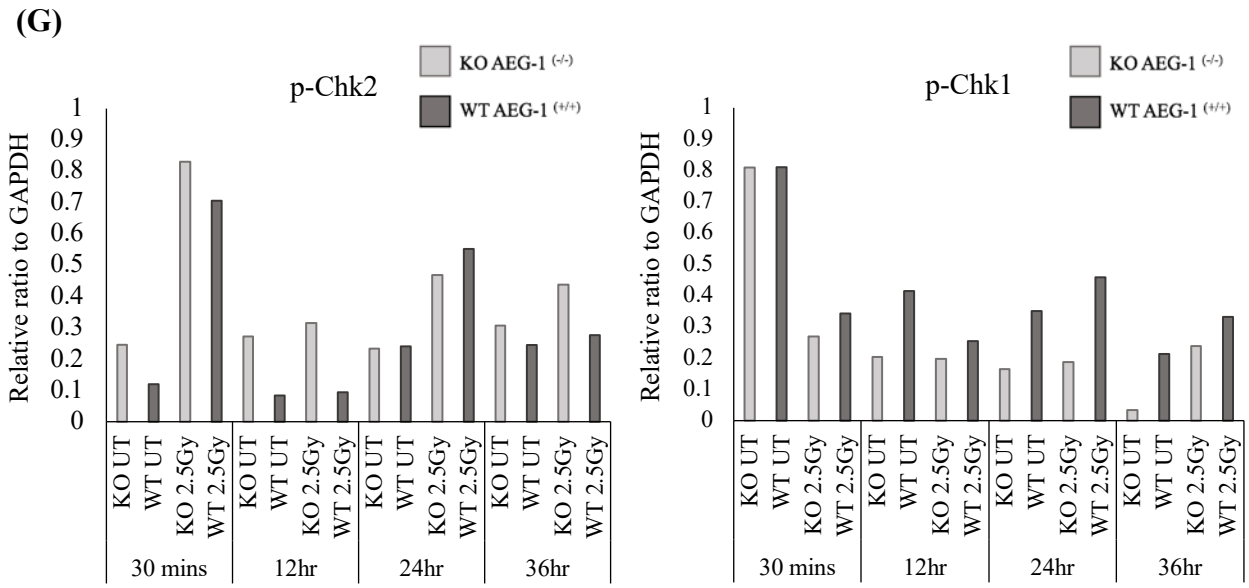

Figure 10 HuH7 cells treated with low-dose IR do not show upregulated p-ATM, p-ATR, or p-BRCA1 signaling, but show upregulation of p-Chk2 and p-Chk1 expression at later time-points. HuH7 cells were collected for whole protein lysate following IR (2.5Gy) or release from double thymidine block (UT) at 30 minutes, 12 hours, 24 hours, and 36 hours. Lysates were then subjected to SDS-PAGE and probed for DDR signaling proteins. (A-C) Western blot images (top) showing expression of total ATM and p-ATM (A), total ATR and p-ATR (B), and p-BRCA1 (C), with quantification of the phosphorylated proteins relative to internal loading controls (bottom). (D-E) Western blot images of p-Chk2 (D), and p-Chk1 (E). (F) Representative western blot images of internal loading controls used for quantification of expression. (G) Quantification of p-Chk2 (left) and p-Chk1 (right) relative to GAPDH.

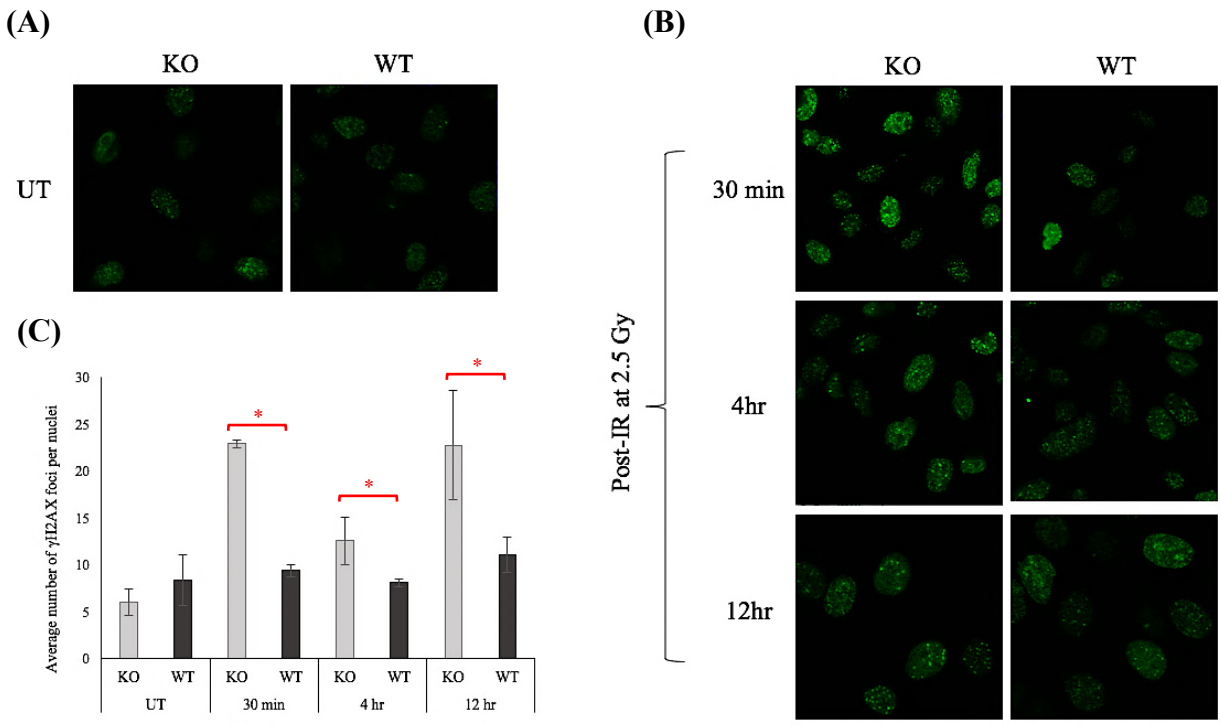

Figure 11 Knockout of AEG-1 induces increased histone H2AX phosphorylation following ionizing radiation. Representative confocal images of QGY-7703 cells stained for γH2AX fluorescence, with either no treatment (A) or ionizing radiation at 2.5 Gy (B). (C) γH2AX foci were quantified using ImageJ by finding maxima in each image. While both AEG-1 KO and WT untreated cells showed a similar number of γH2AX foci, the number of γH2AX foci was persistently and significantly increased in KO cells at all time-points following IR.

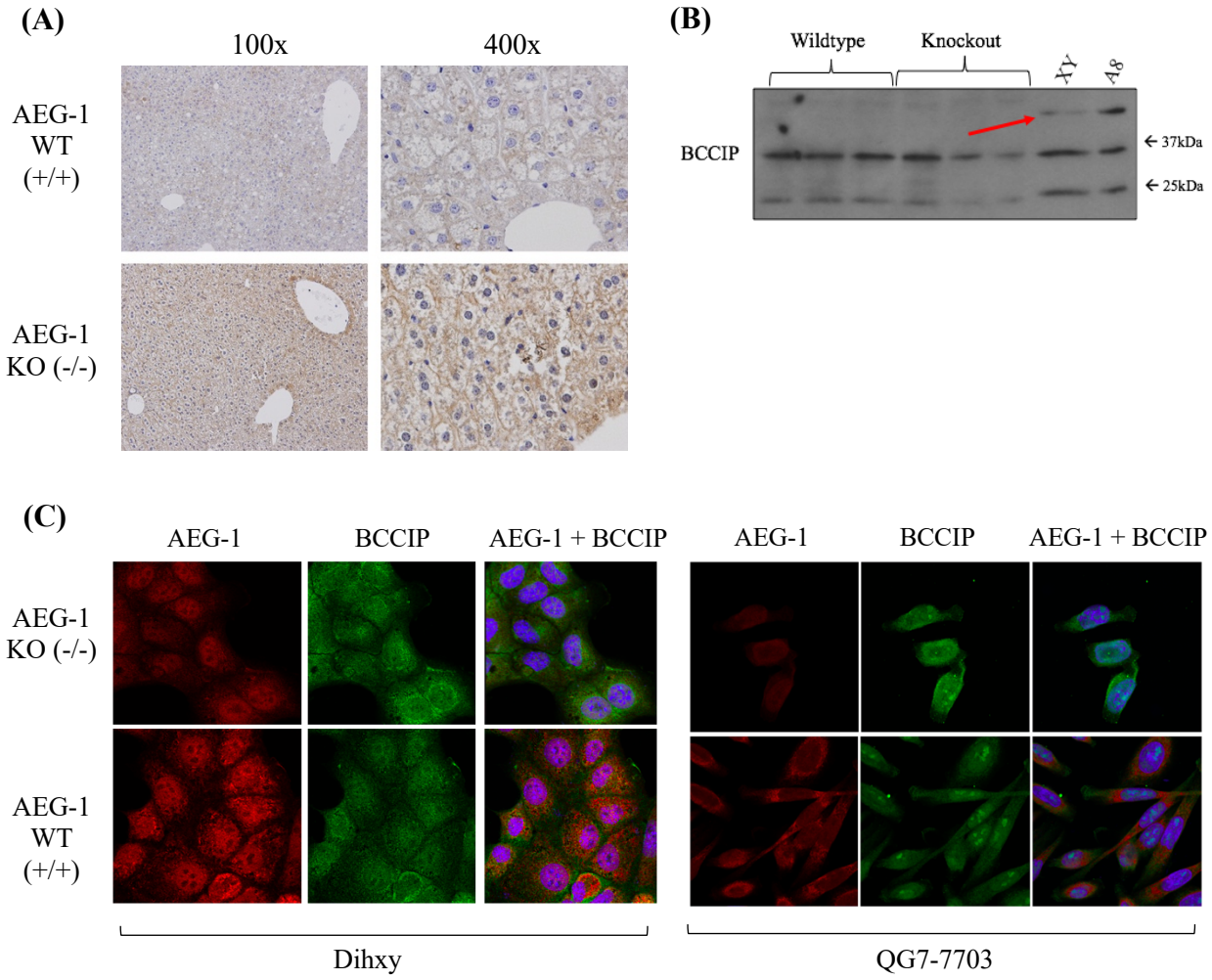

Figure 12 BCCIP expression is upregulated in AEG-1 KO mouse hepatic liver cells, but not in DihXY or QGY-7703 AEG-1 KO cells. (A) Immunohistochemistry staining of mouse hepatic liver cells, stained with anti-BCCIP antibody. (B) Western blot probed for BCCIP in mouse hepatic whole protein lysates. Lanes 1-3 are wildtype for AEG-1; lanes 4-6 are AEG-1 KO; lane 7 is DihXY wildtype for AEG-1; lane 8 is DihXYA8 knockout of AEG-1. (C) Representative immunofluorescence confocal images of DihXY cells (left) and QGY-7703 cells (right) stained with anti-AEG-1 (red), anti-BCCIP (green), and DAPI (blue).

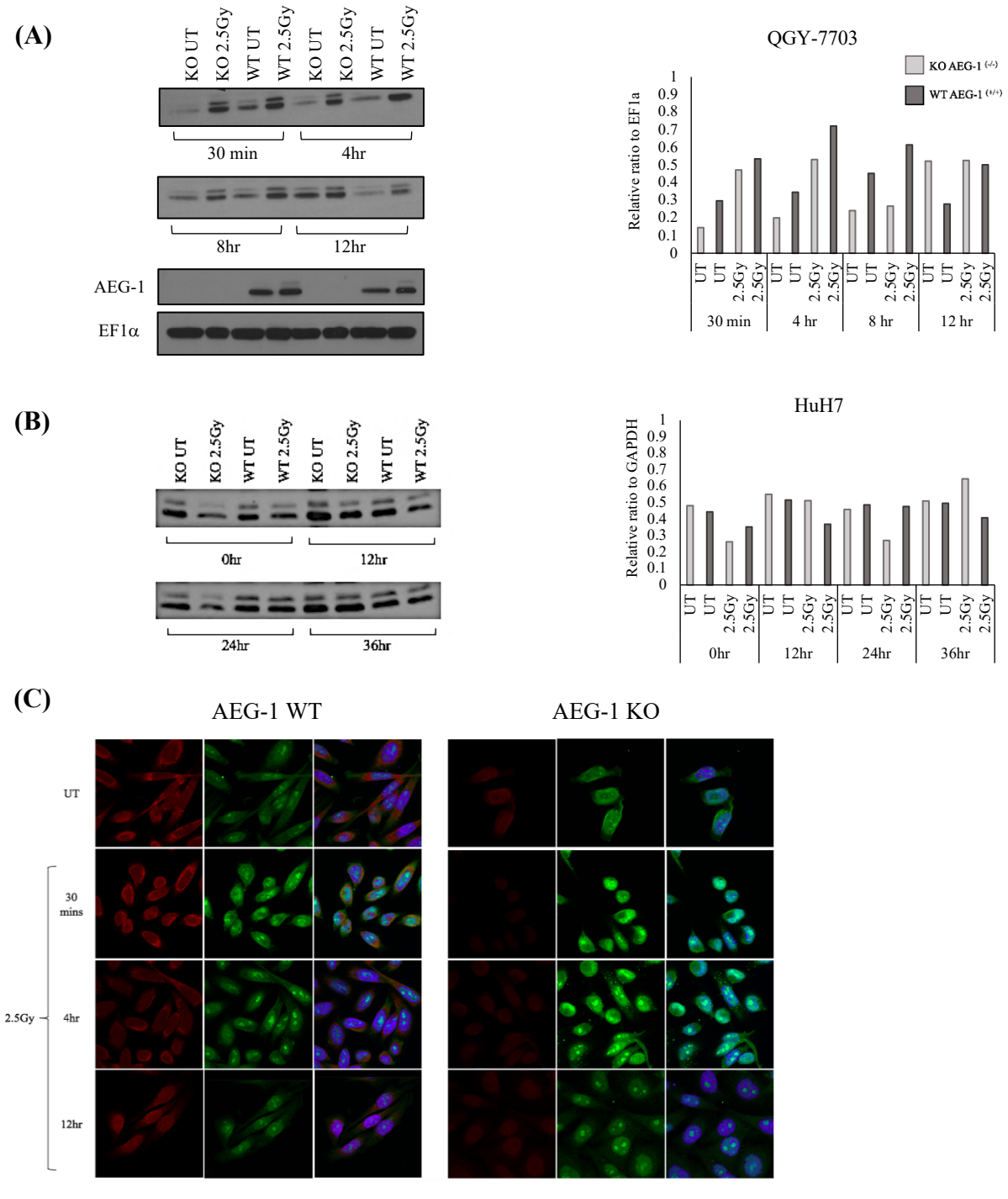

Figure 13 BCCIP expression is upregulated following ionizing radiation at 2.5 Gy in QGY-7703, but not HuH7, cells. (A) QGY-7703 AEG-1 KO and WT cells were collected at 30 mins, 4 hours, 8 hours, and 12 hours following either release from a double thymidine block (UT), or treated with 2.5 Gy and then assessed for BCCIP expression via western blotting. Protein expression was then quantified (right) relative to EF1α expression. (C) Representative confocal images of cells to detect BCCIP immunofluorescence in QGY-7703 UT and irradiated cells. UT cells were not synchronized for IF imaging. Cells were stained with AEG-1 (red), BCCIP (green), and DAPI (blue).

CHAPTER 5

DISCUSSION

HCC is a highly lethal disease and its limited treatment options are discouraging for advanced-stage patients with non-resectable tumors. Resistance to the targeted kinase inhibitor, Sorafenib, and to radiation therapy makes the situation even more grim. Regorafenib (Stivarga®) has been the only targeted therapy to be approved for treatment of HCC patients in recent years, and is used in the context of patients whose tumors worsen during or after sorafenib treatment.

In recent years, targeted gene therapy is becoming increasingly focused on as a method of overcoming issues with chemoresistance and radioresistance in multiple cancer types. However, phase III clinical trials using various targeted therapies in HCC patients have failed due to induced liver toxicity, low efficacy, or heterogeneity in the molecular background of HCC tumors. Targeting AEG-1 mRNA expression with a nanoparticle-delivery system has shown significant growth inhibition of orthotopic human xenografts in mice, indicating the protein could be a promising molecular target for treating HCC patients[48].

AEG-1 has been shown to be involved in the activation of numerous growth-promoting pathways, is potently upregulated in HCC, and promotes hepatocarcinogenesis in both *in vitro* and *in vivo* models[10,14,16]. The results from cell proliferation, invasion, and migration studies in the present study confirm the already well-characterized phenotypic effects of AEG-1 upregulation. In HuH7 and QGY-7703 cells with deficient AEG-1 expression, there was a significant decrease in *in vitro* matrigel invasion and wound closure. These assays are well-established methods to replicate the epithelial mesenchymal transition of carcinogenesis, which is the process by which tumor cells metastasize outside of the primary tumor site[49]. In the QGY-7703 cell line, there was also a significant reduction of AEG-1 KO cell survival in the colony

formation assay, and a significant reduction in cell viability of AEG-1 KO cells in the MTT assay. Although we did not observe reduced cell viability and cell survival in the HuH7 AEG-1 KO cell line, the KO cells showed significantly lower migration and invasion, which eliminates cell proliferation as a confounding variable in the wound closure and matrigel invasion assays. Furthermore, in the growth curve of the HuH7 cells, AEG-1 WT cells exhibit a sharp increase in cell proliferation after 2 days of incubation. An explanation for these conflicting results is that the HuH7 and QGY-7703 KO cell lines are phenotypically different from each other in their capacity to proliferate due to the variability inherent in picking random clones produced from CRISPR/Cas9. Regardless, from these results, and from western blot imaging of AEG-1 expression, we were confident that AEG-1 knockout was established in the cell line and was producing the expected phenotypic effects.

Because cell proliferation was significantly reduced in the QGY-7703 AEG-1 KO cells, we reasoned that cell cycle progression must also be delayed in the KO cell line. In maintenance of the cell lines, QGY-7703 cells become confluent at least 1-2 days sooner than HuH7 or DihXY cells. Double-thymidine block and cell cycle characterization have also previously been established in the QGY-7703 cell line[50]. We therefore chose to use 0, 4, 8, and 12 hours as time-points for cell cycle analysis in the QGY-7703 cell line. DihXY cells become confluent approximately one day slower than QGY-7703 cells, and so 0, 4, 8, 12, 16, and 24 hours cell cycle time-points were chosen for the this study. Finally, HuH7 cells reach confluency slowest among the cell lines. We initially collected HuH7 cells every 6 hours for 48 hours for cell cycle analysis (data not shown). Upon analysis, we identified that HuH7 cells complete a full cell cycle at 36 hours. Subsequently, 0, 12, 24, and 36 hours were chosen for cell cycle analysis. Across the DihXY, HuH7, and QGY-7703 cell lines, cell cycle progression was consistently reduced at all

chosen time-points in the AEG-1 knockout clones. This deceleration in cell cycle progression was more readily apparent in the QGY-7703 AEG-1 KO cells than in the other cell lines. One explanation for this observation is that AEG-1 is expressed to a much higher degree in the QGY-7703 AEG-1 WT cells compared to the HuH7 AEG-1 WT cells (see Yoo et al. 2009, Fig. 1A[11]), indicating QGY-7703 cells may be more addicted to AEG-1 expression and therefore proliferate faster.

The present study identifies AEG-1 as a potential target in sensitizing radioresistant HCC tumors to radiation treatment. By using three different cell lines modeling HCC, we have shown that knockout of AEG-1 promotes sensitization to radiation at a clinically relevant dosage of 2.5Gy. While ionizing radiation at 10Gy proved completely cytotoxic to both AEG-1 WT and KO cells across all cell lines, there was a significant reduction in cell viability in AEG-1 KO cells treated with 2.5Gy. These results prompted us to assess protein expression of cell cycle regulatory molecules and of signaling and effector molecules involved in the DNA damage response pathway.

Appropriate DNA replication, cell cycle progression, and mitosis are all required for accurate chromosome segregation and maintenance of genomic stability. Normally, cells that fail to abide by these tightly regulated pathways are directed to apoptosis; however, cancer cells can finetune expression of oncogenes or tumor suppressor genes to persist despite errors in mitosis or cell cycle checkpoints. BCCIP is one of many proteins involved in the G1/G0 transition in the cell cycle, along with spindle pole stabilization during mitosis. We were initially interested in studying BCCIP expression in the context of AEG-1 knockout due to evidence that BCCIPα directly interacts with AEG-1 in prostate tumor cells. Furthermore, Ash et al. provided evidence that AEG-1 overexpression leads to proteasomal degradation of BCCIP, suggesting a potential

role of AEG-1 expression in abrogating the G1/S checkpoint[44]. Although we observed increased anti-BCCIP staining in IHC of AEG-1 KO mouse hepatic tissue samples compared to AEG-1 WT samples, we did not observe this difference in IF staining of DihXY or QGY-7703 cells. BCCIP appeared to be primarily localized to the nucleus with faint signaling in the cytoplasm, as seen in the DAPI-merged IF images. This localization is consistent with prior evidence that both BCCIPα and BCCIPβ are localized to the nucleus under confocal microscopy[37]. Furthermore, we did not observe a noticeable change in BCCIP localization in either the untreated or irradiated AEG-1 WT QGY-7703 cells. The present study therefore provides new evidence that BCCIP localization is not affected by ionizing radiation in HCC cells.

After observing conflicting evidence of BCCIP signaling in IHC and IF assays, we sought to analyze BCCIP protein expression in untreated and irradiated HCC cells. Unexpectedly, BCCIP expression was increased in QGY-7703 AEG-1 WT cells at all time-points except for 12 hours post-thymidine release, when compared to AEG-1 KO cells. Although FACS analysis of both WT and KO cells at 12 hours show accumulation in G1/G0 phase, this decrease in BCCIP expression in AEG-1 WT cells indicates a lack of G1/S checkpoint in the WT cells as they continue unrestricted proliferation, which corroborates prior evidence that downregulation of BCCIP in hepatocytes promotes G1/S transition and increases cell proliferation[39]. On the other hand, BCCIP expression in the untreated HuH7 cell line was minimally upregulated in AEG-1 KO cells compared to WT cells at all time-points, except 24 hours, actually confirming the findings of Ash et al[44]. Furthermore, BCCIP expression was markedly increased in the AEG-1 WT cells of both QGY-7703 and HuH7 cell lines at 30 minutes post-IR, but its expression was in fact downregulated in the HuH7 cells, while upregulated in the QGY-7703 cells, compared to their untreated counterparts, at this initial time-point. This conflicting pattern of BCCIP

expression in the QGY-7703 and HuH7 AEG-1 WT cell lines may be attributed to the *TP53* mutational status of the HuH7 cell line. While QGY-7703 cells contain wildtype *TP53*, HuH7 cells overexpress a mutant p53 that exhibits a longer half-life – when compared to p53 of other HCC cell lines and to normal liver cells – due to a point mutation in the coding region of *TP53*[51,52].

Because BCCIP has roles in both cell cycle regulation and homologous recombination repair, it is difficult to attribute the upregulation of BCCIP in the irradiated QGY-7703 AEG-1 WT cells to a specific pathway. Hence, the expression of BCCIP cannot be examined in a compartmentalized manner. In a more comprehensive view of proteins involved in the DNA damage response, we observed stronger, more rapid expression of p-ATM, p-ATR, and γH2AX – all involved in signaling for initiation of homologous recombination repair – in the irradiated AEG-1 WT cells than in the AEG-1 KO cells. Although p-ATM, γH2AX, and p-ATR in QGY-7703 signaling in AEG-1 WT cells was initially stronger (30 minutes post-IR) compared to AEG-1 KO cells, the expression pattern switched at subsequent time-points to be increased in AEG-1 KO cells compared to WT cells. Similarly, p-BRCA1 and p-Chk1 expression showed a sharp increase in HuH7 irradiated AEG-1 WT cells at 24 hours post-IR, and their expression was higher in HuH7 irradiated AEG-1 KO cells at 36 hours. Analysis of the downstream checkpoint kinase p-Chk2 showed that its expression was increased in the QGY-7703 AEG-1 WT cells at 30 minutes until 8 hours post-IR at 2.5Gy, after which the irradiated AEG-1 KO cells showed increased expression. This can be explained by an initial, rapid activation of ATM, ATR, BRCA1, and γH2AX signaling, as observed in the AEG-1 WT cells at 30 minutes post-IR, which is subsequently followed by more rapid activation of p-Chk2 and p-Chk1 in the AEG-1 WT cells. Therefore, there is reliable evidence that AEG-1 WT cells induce the DDR more rapidly,

and is a possible mechanism by which DSB's are repaired more efficiently by AEG-1 overexpressing cells to protect HCC from low-dose ionizing radiation.

A potential limitation of our findings is that p-Chk1 and γH2AX signaling can be indicators of the DNA damage response, but are not specific to this process[51]. Immunofluorescence staining of γH2AX is used to demonstrate DDR foci in cells treated with IR. In response to DNA damage, γH2AX is phosphorylated on its Ser139 residue and signals for mediator of DNA damage checkpoint 1 (MDC1) to directly bind γH2AX at its BRCT domain. This is required for recruitment of DDR complexes such as 53BP1 to repair damaged DNA[53,54]. However, H2AX phosphorylation is also implicated in replication stress and checkpoint abrogation[55,56]. Nevertheless, because we also observed an upregulation of p-ATM and p-chk2 expression in conjunction with γH2AX signaling, we provide convincing data that DSB-induced signaling is initiated in QGY-7703 AEG-1 WT cells more rapidly than in KO cells.

In the present study we observed p-ATR expression was upregulated in AEG-1 WT cells after IR at 2.5Gy. In fact, p-ATR expression was consistently upregulated in QGY-7703 AEG-1 WT cells at all time-points following IR at 2.5Gy. The results were not as remarkable in HuH7 AEG-1 WT cells, but we did observe marked, increased upregulation of p-ATR expression at 24 hours post-IR when compared to AEG-1 KO cells. We therefore became interested in the possibility of WT AEG-1 cells protecting cells from low-dose ionizing radiation through increased replication fork stabilization. Cancer cells have higher baseline rates of replication due to oncogenic drivers and therefore may have increased incidence of replicative stress in the absence of genotoxic stressors[52]. In the context of HCC, non-transformed hepatocytes are quiescent and normally

divide only rarely, making them susceptible to replicative stress[57]. Hepatic cells may therefore have increased replication fork protection at a basal level, even prior to carcinogenesis.

DNA replication stress encompasses any endogenous or exogenous stressor that can induce replication fork stalling or damage, generating exposed single-stranded DNA and inducing the intra-S-phase checkpoint. Replication stress is sensed by ATR, which autophosphorylates and relays the signal to the Chk1 effector kinase. BRCA1, BRCA2, and the Fanconi anemia family of proteins are required for MRE11 nuclease to protect nascent DNA strands at stalled replication forks. While they use very similar proteins in their processes, HRR and replication fork protection are functionally separate[58,59]. Topoisomerase IIβ-binding protein 1 (TopBP1) activates ATR and is required for resolving replication stress to prevent formation of 53BP1 nuclear bodies. Ultimately, ATR activation in response to replication stress is fundamental to protect genomic integrity and repair stalled replication forks prior to mitotic entry. Therefore, an intra-S-phase checkpoint is induced while replication forks are repaired in the presence of stress. Replication stress can be a result of too few origins of replication or insufficient activation of these origins; activation of too many origins of replication, which can lead to depletion of histones or DNA binding protein RPA and subsequently the collapse of replication forks. Replication stress can also be induced by exogenous stressors, including UV-light or genotoxic agents - such as hydroxyurea, cisplatin, mitomycin C, and camptothecin. There is also mounting evidence that activation of oncogenes results in replication stress by affecting origin firing, nucleotide depletion, or changing temporal stability of the cell cycle [61,62]. The present findings identify a previously unexplored role of AEG-1 expression in protecting HCC cells from radiation therapy through upregulation of p-ATR. Further investigation needs to be conducted on

AEG-1 in protecting replication forks before we can positively conclude that this is another pathway through which AEG-1 induces radioresistance.

Recently, whole genome sequencing, whole exome sequencing, and RNA-sequencing of 751 distinct HCC tissues identified a subgroup of HCC tumors that contain mutated *CCNE1* (encoding cyclin E) or *CCNA2* (encoding cyclin A2) from patients who developed HCC in a non-cirrhotic background. The lab identified recurrent *CCNA2* fusions and *CCNE1* promoter region rearrangements[60]. Cancers with such mutational backgrounds are characterized by high amounts of replication stress due to increased proliferation rates[62]. The present study showed cyclin E upregulation in untreated HuH7 AEG-1 KO cells at 12, 24, and 36 hours post-thymidine release, and in irradiated AEG-1 KO cells at 30 minutes, 12, and 36 hours post-IR at 2.5Gy. On the other hand, cyclin E protein expression was upregulated in untreated QGY-7703 AEG-1 WT cells at 30 minutes and 4 hours post-thymidine release, while AEG-1 KO cells had increased expression at 8 and 12 hours. In both AEG-1 WT and KO QGY-7703 cells, cyclin E was consistently upregulated at all time-points at both 2.5 and 10Gy dosages. Cyclin E expression patterns in QGY-7703 cells, along with our observations of upregulated p-ATR signaling in QGY-7703 cells across all time-points, is consistent with prior reports that cyclin E upregulation is associated with ATR upregulation in HCC[64]. Furthermore, evidence in our study of both cyclin E and p-ATR overexpression in irradiated QGY-7703 cells point to induction of replication stress in these cells in response to IR, as cyclin E regulation is implicated in appropriate origin of replication firing[55].

Along the same line of reasoning, our observations of cyclin E upregulation, yet slowed cell cycle progression, in the irradiated QGY-7703 cells can be attributed to p-Chk2 upregulation. P-Chk2 has been shown to inhibit enzymatic activity of the cyclin E/Cdk2 complex[21]. As we

observed a strong increase in p-Chk2 expression in the irradiated QGY-7703 cells, there is a possibility that p-Chk2 is interacting with the cyclin E/Cdk2 complex to delay cell cycle progression, while transcription of *CC2NE1* is upregulated.

An unexpected finding of this study was upregulation of AEG-1 expression in QGY-7703 cells in response to ionizing radiation, as was evidenced by both western blot analysis and confocal microscopy. A current literature search only shows one prior study of AEG-1 expression in the context of ionizing radiation. However, this study focused on preventing recurrence of distant metastatic tumors in rectal cancer patients through AEG-1 knockdown[66]. The present study therefore provides evidence that AEG-1 itself is upregulated in response to ionizing radiation in HCC cells, along with affecting protein expression of DDR kinases. There are multiple ways through which protein expression of AEG-1 is upregulated in HCC: genomic amplification, post-translational monoubiquitination, transcriptional activation by c-myc, downregulation of miR-375, and/or binding of cytoplasmic polyadenylation element-binding protein 1 (CPEB1) to AEG-1 mRNA to activate its translation[67,68]. The mechanism by which AEG-1 is upregulated following IR treatment can be the focus of a future project.

A limitation of the present study is that use of the CRISPR/Cas9 system to knockout a gene comes with several drawbacks. One of these drawbacks is potential off-target effects that the vector may induce in the selected clones. Until full genomic profiling is conducted on the cell lines, the possibility of insertional or deletion mutations in genes other than the intended target, AEG-1, must be considered. Furthermore, the clones selected for these studies are randomly generated and selected, and each clone may be slightly phenotypically or genetically different from another. However, as previously described, AEG-1 expression can be upregulated in a number of ways, including through genomic amplification. Complete deletion of the gene in

three diverse HCC cell lines was a feat in and of itself, and has provided considerable critical insight needed to address the aims established for this project. These concerns can be addressed, and the results of this study validated, by selecting multiple AEG-1 knockout clones from each cell line in future projects, or replicating the results *in vivo* using the Cre/*lox* conditional knockout system to abrogate AEG-1 expression.

We conclude that AEG-1 expression protects HCC cells from low-dose ionizing radiation through two mechanisms: 1) initiating the DNA damage response rapidly and efficiently; and 2) increasing replication fork stabilization in the face of replication stress. The scope of this study did not fully address the mechanistic role of AEG-1 expression in resolving stalled replication forks or in promoting more rapid DSB repair, and therefore needs to be clarified in future studies. Regardless, the results described here do give us a promising method of sensitizing radioresistant HCC tumors through abrogation of AEG-1 expression.

CHAPTER 6

FUTURE DIRECTIONS

Although our results are exciting, they must be replicated *in vivo* to establish validity in their ability to be translated to the clinic. A Cre/*lox* model of liver-specific AEG-1 knockout in mice, with subsequent DEN-induced liver tumor formation, can be used to demonstrate replicability of sensitization to ionizing radiation in AEG-1 deficient HCC cells. Another viable method would be to use nanoparticle delivery of AEG-1 siRNA (as described by Rajasekaran et al. 2015[48]) in combination with radiation therapy in mice containing xenografts of QGY-7703 or HuH7 parental cell lines[48].

A major question we are left with after the results described here is whether p-ATR upregulation induced by AEG-1 expression in irradiated HCC cells is due to replication fork stabilization. Activated ATR has diverse functions in both DSB and SSB repair; therefore, it is crucial that we identify in which functional pathway p-ATR is being used to protect HCC cells from IR. There are several ways to identify activation of the replication stress response. Possibly the simplest method is the cell cycle restart assay, in which cells are treated with hydroxyurea to deplete dNTP's. Other methods involve quantification of replication foci or origins. IF staining of IdU – a thymidine analog – can be used to quantify replication foci in early S-phase cells. Additionally, DNA fiber analysis quantifies firing of replication origins and distances between origins[69]. A more complex but comprehensive method would be to analyze the genetic expression patterns of replication-stress-associated genes in both untreated and irradiated AEG-1 KO and WT cells. A recent paper used a cell line with diminished ATR expression to generate a replication stress defect signature through microarray analysis. A similar model could be created by knockdown of

ATR, via short hairpin RNA, in HuH7 and QGY-7703 cell lines to compare against the replication stress gene signature of irradiated cells[70].

Several inhibitors that target proteins involved in the cell cycle have been previously studied in HCC models. The Wee1 kinase inhibitor AZD1775 has recently been shown to sensitize HCC cells to radiation treatment. Wee1 is a Ser/Thr kinase that was originally identified in the fission yeast *S. pombe*. The human homologues for *Wee1* are *Wee1A* and *Wee1B*. Wee1 kinase is involved in G2 checkpoint regulation and replication initiation via inhibition of CDK1, and Wee1 kinase activity is implicated in preventing replication stress and inappropriate DNA replication. In Hep3B and HuH7 HCC cell lines, Cdk1 phosphorylation – which is an indicator of G2 arrest – was increased when treated with ionizing radiation, but this arrest was absent when radiation was combined with AZD1775 treatment[44]. Another recent paper has also reviewed evidence that a combination of ATR and Wee1 kinase inhibitors can target both replication fork stabilization and HRR in cancerous cells[29]. Although phase I and II clinical trials are currently underway to target *ATR, CHK1*, and *WEE1*, these are not being studied in the context of HCC[62]. Therefore, a study using a panel of ATR, Wee1, and Chk1 kinase inhibitors in our model can provide insight as to whether knockout of AEG-1 induces increased sensitivity of HCC cells to these inhibitors, as well as provide rationale for using such inhibitors in an *in vivo* model of HCC. The results could also clue us into how AEG-1 interacts with these diverse signaling proteins to induce radioresistance.

Aurora kinases are serine/threonine kinases involved in maintaining appropriate cell cycle progression and genomic stability. Inhibiting aurora kinases induces a postmitotic checkpoint and accumulates cells in a pseudo-G1 state that requires p53. Prior studies have shown aggressive HCC with poor prognosis correlated with overexpression of aurora kinases A and

B[71,72]. The same lab that identified Aurora kinases A and B overexpression in HCC then showed that HCC can be sensitized to radiation when treated with the broad aurora kinase inhibitor VE-465[73]. Although expression of aurora kinases were not analyzed in the present study, observing the effect of wide-spectrum aurora kinase inhibition in an AEG-1 KO model could be another avenue of investigating how AEG-1 interacts with cell cycle regulators.

In addition, the exact mechanism through which AEG-1 interacts with the DNA damage response is still unclear. AEG-1 is a potent upregulator of the PI3K/Akt and RAF-1-MEK1/2-ERK1/2 pathways. These signaling pathways are pro-survival and have been shown to be activated in response to ionizing radiation in various cancer cell types. Ionizing radiation at low, clinically-relevant doses (1-2 Gy) induces phosphorylating activation of epidermal growth factor receptors ERBB1 and HER1 due to generation of reactive oxygen species and reactive nitrogen species in the mitochondria, which reduce protein tyrosine phosphatase activity of ERBB1 and HER1. This reaction occurs during the initial response to ionizing radiation. Following several hours, it is hypothesized that ERK1/2 and Akt signaling can change cyclin expression profiles, along with affecting levels of pro-cell survival molecules Bcl-2, Bcl-XL, MCL-1, c-FLIP, XIAP, IAP1, and pro-apoptotic molecules BAD and BIM. This in turn allows for survival of a small subset of the cell population to continue actively proliferating despite radiation treatment[74,75,76]. There is also evidence that tumors containing *H-RAS, K-RAS*, or *N-RAS* mutations may also be protected from ionizing radiation because they too can activate the PI3K pathway inappropriately. Targeting PI3K signaling using small molecule inhibitors sensitizes these tumor cells to ionizing radiation[77]. In order to discern whether knockout of AEG-1 itself has a functional effect on reducing the DNA damage response, or if dampening of PI3K/Akt/ERK1/2 signaling as a result of AEG knockout induces sensitization to radiation treatment, it would be

prudent to repeat the radiation studies in *in vitro* models with depletion of PI3K/Akt signaling in AEG-1 WT clones, or reconstitution of the pathway in AEG-1 KO clones.

Finally, because our findings of BCCIP expression in the context of AEG-1 expression conflict with both the literature[44] and within our study between the QGY-7703 and HuH7 cell lines, it is evident that replicating Ash et al.'s co-immunoprecipitation of AEG-1 with BCCIP must be conducted in multiple HCC cell lines. Further investigation of this interaction between AEG-1 and BCCIP can clarify the role of BCCIP function in the context of AEG-1 overexpressing HCC cells, as well as identify possible heterogeneity in their interaction across various HCC cell lines.

REFERENCES

1. F. Bray, Ferlay J, Soerjomataram I, Siegel R, Torre L, Jemal A. Global cancer statistics 2018: GLOBOCAN estimates of incidence and mortality worldwide for 36 cancers in 185 countries. *Cancer J Clin*. 2018;68(6):394-424. doi:doi:10.3322/caac.21492

2. El-Serag H. Epidemiology of Viral Hepatitis and Hepatocellular Carcinoma. *Gastroenterology*. 2012;142(6):1264–1273. doi:10.1053

3. Grazie M, Biagini M, Tarocchi M, Polvani S, Galli A. Chemotherapy for hepatocellular carcinoma: The present and the future. *World J Hepatol*. 2017;9(21):907-952. doi:10.4254/wjh.v9.i21.907

4. Daher S, Massarwa M, Benson A, Khoury T. Current and Future Treatment of Hepatocellular Carcinoma: An Updated Comprehensive Review. *J Clin Transl Hepatol*. 2018;6:69-78. doi:10.14218/JCTH.2017.00031

5. Hawkins M, Dawson L. Radiation therapy for hepatocellular carcinoma. *Cancer*. 2006;106(8):1653-1663. doi:doi:10.1002/cncr.21811

6. Wang P, Hsu W, Chung N, Chang F, Fogliata A, Cozzi L. Radiation treatment with volumetric modulated arc therapy of hepatocellular carcinoma patients. Early clinical outcome and toxicity profile from a retrospective analysis of 138 patients. *Radiat Oncol*. 2012;7(1):207-215. doi:10.1186/1748-717x-7-207

7. Mornex F, Girard N, Beziat C, et al. Feasibility and efficacy of high-dose three-dimensional-conformal radiotherapy in cirrhotic patients with small-size hepatocellular carcinoma non-eligible for curative therapies—mature results of the French Phase II RTF-1 trial. *Int J Radiat Oncol*. 2006;66(4):1152-1158. doi:10.1016/j.ijrobp.2006.06.015

8. Yu Y, Feng M. Radiotherapy for Hepatocellular Carcinoma. *Semin Radiat Oncol*. 2018;28(4):277-287. doi:10.1016/j.semradonc.2018.06.005

9. Su Z-Z, Chen Y, Kang D, et al. Customized rapid subtraction hybridization (RaSH) gene microarrays identify overlapping expression changes in human fetal astrocytes resulting from human immunodeficiency virus-1 infection or tumor necrosis factor-α treatment. *Gene*. 2003;306:67-78. doi:10.1016/s0378-1119(03)00404-9

10. Su Z-Z, Kang D, Chen Y, et al. Identification and cloning of human astrocyte genes displaying elevated expression after infection with HIV-1 or exposure to HIV-1 envelope glycoprotein by rapid subtraction hybridization, RaSH. *Oncogene*. 2002;21(22):3592-3602. doi:10.1038/sj.onc.1205445

11. Yoo B, Emdad L, Su Z-Z, et al. Astrocyte elevated gene-1 regulates hepatocellular carcinoma development and progression. *J Clin Invest*. 2009;119(3):465-477. doi:10.1172/jci36460

12. Srivastava J, Siddiq A, Emdad L, et al. Astrocyte elevated gene-1 promotes hepatocarcinogenesis: Novel insights from a mouse model. *Hepatology*. 2012;56(5):1782-1791. doi:10.1002/hep.25868

13. Kang D, Su Z-Z, Sarkar D, Emdad L, Volsky D, Fisher P. Cloning and characterization of HIV-1-inducible astrocyte elevated gene-1, AEG-1. *Gene*. 2005;353(1):8-15. doi:10.1016/j.gene.2005.04.006

14. Srivastava J, Robertson C, Rajasekaran D, et al. AEG-1 Regulates Retinoid X Receptor and Inhibits Retinoid Signaling. *Cancer Res*. 2014;74(16):4364-4377. doi:10.1158/0008-5472.can-14-0421

15. Sarkar D, Park E, Emdad L, Lee S, Su Z-Z, Fisher P. Molecular Basis of Nuclear Factor-kappaB Activation by Astrocyte Elevated Gene-1. *Cancer Res*. 2008;68(5):1478-1484. doi:10.1158/0008-5472.can-07-6164

16. Yoo B, Emdad L, Lee S, et al. Astrocyte elevated gene-1 (AEG-1): A multifunctional regulator of normal and abnormal physiology. *Pharmacol Ther*. 2011;130(1):1-8. doi:10.1016/j.pharmthera.2011.01.008

17. Robertson C, Srivastava J, Siddiq A, et al. Genetic Deletion of AEG-1 Prevents Hepatocarcinogenesis. *Cancer Res*. 2014;74(21):6184-6193. doi:10.1158/0008-5472.can-14-1357

18. Sotillo E, Grana X. Escape from Cellular Quiescence. In: *Cell Cycle Deregulation in Cancer*. ; 2010. 10.1007/978-1-4419-1770-6_1.

19. Sherr C. Mammalian G1 cyclins. *Cell*. 1993;73(6):1059-1065. doi:10.1016/0092-8674(93)90636-5

20. Morgan D. Principles of CDK regulation. *Nature*. 1995;374:131-134. doi:10.1038/374131a0

21. Deckbar D, Jeggo P, Lobrich M. Understanding the limitations of radiation-induced cell cycle checkpoints. *Crit Rev Biochem Mol Biol*. 2011;46(4):271-283. doi:10.3109/10409238.2011.575764

22. Yasutis K, Kozminski K. Cell cycle checkpoint regulators reach a zillion. *Cell Cycle*. 2013;12(10):1501-1509. doi:10.4161/cc.24637

23. Kawabe T. G2 checkpoint abrogators as anticancer drugs. *Mol Cancer Ther*. 2004;3:513-519. doi:PMID:15078995

24. Sherr C, Roberts J. Inhibitors of mammalian G1 cyclin-dependent kinases. *Genes Dev*. 1995;9(10):1149-1163. doi:10.1101/gad.9.10.1149

25. Azzam E, Jay-Gerin J, Pain D. Ionizing radiation-induced metabolic oxidative stress and prolonged cell injury. *Cancer Lett*. 2012;327(1-2):48-60. doi:10.1016/j.canlet.2011.12.012

26. Moeller B, Pasqualini R, Arap W. Targeting cancer-specific synthetic lethality in double-strand DNA break repair. *Cell Cycle*. 2009;8(12):1872-1876. doi:10.4161/cc.8.12.8743

27. Savage K, Harkin D. BRCA1, a 'complex' protein involved in the maintenanceof genomic stability. *FEBS J*. 2015;282:630-646. doi:10.1111/febs.13150

28. Lomonosov M, Anand S, Sangrithi M, Davies R, Venkitaraman A. Stabilization of stalled DNA replication forks by the BRCA2 breast cancer susceptibility protein. *Genes Dev*. 2003;17(24):3017-3022. doi:10.1101/gad.279003

29. Haynes B, Murai J, Lee J-M. Restored replication fork stabilization, a mechanism of PARP inhibitor resistance, can be overcome by cell cycle checkpoint inhibition. *Cancer Treat Rev*. 2018;71:1-7. doi:10.1016/j.ctrv.2018.09.003

30. Nam E, Cortez D. ATR signaling: more than meeting at the fork. *Biochem J*. 2011;436(3):527-536. doi:10.1042/BJ20102162

31. Venkitaraman A. Cancer suppression by the chromosome custodians, BRCA1 and BRCA2. *Science*. 2014;343(6178):1470-1475. doi:10.1126/science.1252230

32. Fisher A, Hochegger H, Takeda S, Cadecott K. Poly(ADP-ribose) polymerase 1 accelerates single-strand break repair in concert with poly(ADP-ribose) glycohydrolase. *Mol Cell Biol*. 2007;27(15):5597-5605. doi:10.1128/MCB.02248-06

33. Haince H, Kozlov S, Dawson V, et al. Ataxia telangiectasia mutated (ATM) signaling network is modulated by a novel poly(ADP-ribose)-dependent pathway in the early response to DNA-damaging agents. *J Biol Chem*. 2007;282(22):16441–16453. doi:10.1074/jbc.M608406200

34. Fridman J, Lowe S. Control of apoptosis by p53. *Oncogene*. 2003;22(56):9030-9040. doi:10.1038/sj.onc.1207116

35. Caron R, Yacoub A, Mitchell C, et al. Radiation-stimulated ERK1/2 and JNK1/2 signaling can promote cell cycle progression in human colon cancer cells. *Cell Cycle*. 2004;4(3):456-464.

36. Criswell T, Beman M, Araki S, et al. Delayed Activation of Insulin-like Growth Factor-1 Receptor/Src/MAPK/Egr-1 Signaling Regulates Clusterin Expression, a Pro-survival Factor. *J Biol Chem*. 2005;280:14212-14221. doi:10.1074/jbc.M412569200

37. Ono T, Kitaura H, Ugai H, et al. TOK-1, a Novel p21Cip1-binding Protein That Cooperatively Enhances p21-dependent Inhibitory Activity toward CDK2 Kinase. *J Biol Chem*. 2000;275(40):31145-31154. doi:10.1074/jbc.m003031200

38. Meng X, Liu J, Shen Z. Genomic structure of the human BCCIP gene and its expression in cancer. *Gene*. 2003;302(1-2):139-146. doi:10.1016/s0378-1119(02)01098-3

39. Lin Z, Hu B, Ni W, et al. Expression pattern of BCCIP in hepatocellular carcinoma is correlated with poor prognosis and enhanced cell proliferation. *Tumour Biol*. 2016;37(12):16305-16315. doi:10.1007/s13277-016-5424-0

40. Meng X, Lu H, Shen Z. BCCIP Functions through p53 to Regulate the Expression of p21Waf1/Cip1. *Cell Cycle*. 2004;3(11):1457-1462. doi:10.4161/cc.3.11.1213

41. Huhn S, Liu J, Ye C, et al. Regulation of spindle integrity and and mitotic fidelity by BCCIP. *Oncogene*. 2017;36:4750-4766. doi:10.1038/onc.2017.92

42. Lu H, Guo X, Meng X, et al. The BRCA2-interacting protein BCCIP functions in RAD51 and BRCA2 focus formation and homologous recombinational repair. *Mol Cell Biol*. 2005;25(5):1949-1957. doi:10.1128/mcb.25.5.1949-1957.2005

43. Lu H, Yue J, Meng X, Nickoloff J, Shen Z. BCCIP regulates homologous recombination by distinct domains and suppresses spontaneous DNA damage. *Nucleic Acids Res*. 2007;35(21):7160-7170. doi:10.1093/nar/gkm732

44. Ash S, Yang D, Britt D. LYRIC/AEG-1 overexpression modulates BCCIPα protein levels in prostate tumor cells. *Biochem Biophys Res Commun*. 2008;371(2):333-338. doi:10.1016/j.bbrc.2008.04.084

45. Robertson C, Srivastava J, Siddiq A, et al. Astrocyte Elevated Gene-1 (AEG-1) Regulates Lipid Homeostasis. *J Biol Chem*. 2015;290(29):18227-18236. doi:10.1074/jbc.M115.661801

46. Robertson C, Mendoza R, Jariwala N, et al. Astrocyte Elevated Gene-1 Regulates Macrophage Activation in Hepatocellular Carcinogenesis. *Cancer Res*. 2018;78(22):6436-6446. doi:10.1158/0008-5472.CAN-18-0659

47. Spruck CH, Won KA, Reed SI. Deregulated cyclin E induces chromosome instability. *Nature*. 1999;401(6750):297-300. doi:10.1038/45836

48. Rajasekaran D, Srivastava J, Ebeid K, et al. Combination of Nanoparticle-Delivered siRNA for Astrocyte Elevated Gene-1 (AEG-1) and All-trans Retinoic Acid (ATRA): An Effective Therapeutic Strategy for Hepatocellular Carcinoma (HCC). *Bioconjug Chem*. 2015;26:1651-1661. doi:10.1021/acs.bioconjchem.5b00254

49. Justus C, Leffler N, Ruiz-Echevarria M, Yang L. In vitro Cell Migration and Invasion Assays. *J Vis Exp*. 2014;88. doi:10.3791/51046

50. Santhekadur P, Rajasekaran D, Siddiq A, et al. The transcription factor LSF: a novel oncogene for hepatocellular carcinoma. *Am J Cancer Res*. 2012;2(3):269-285.

51. Cuneo K, Morgan M, Davis M, et al. Wee1 Kinase Inhibitor AZD1775 Radiosensitizes Hepatocellular Carcinoma Irrespective of TP53 Mutational Status through the Induction of Replication Stress. *Int J Radiat Oncol*. 2016;95(2):782-790. doi:10.1016/j.ijrobp.2016.01.028

52. Bressac B, Galvin KM, Liang TJ, Isselbacher KJ, Wands JR, Ozturk M. Abnormal structure and expression of p53 gene in human hepatocellular carcinoma. *Proc Natl Acad Sci USA*. 1990;87(5):1973-1977.

53. Rogakou E, Pilch D, Orr A, Ivanova V, Bonner W. DNA Double-stranded Breaks Induce Histone H2AX Phosphorylation on Serine 139. *J Biol Chem*. 1998;273(10):5858-5868. doi:10.1074/jbc.273.10.5858

54. Solier S, Pommier Y. The nuclear γ-H2AX apoptotic ring: implications for cancers and autoimmune diseases. *Cell Mol Life Sci*. 2014;71(12):2289-2297. doi:10.1007/s00018-013-1555-2

55. Murga M, Bunting S, Montana M, et al. A mouse model of ATR-Seckel shows embryonic replicative stress and accelerated aging. *Nat Genet*. 2009;41(8):891-899. doi:10.1038/ng.420

56. Ewald B, Sampath D, Plunkett W. H2AX phosphorylation marks gemcitabine-induced stalled replication forks and their collapse upon S-phase checkpoint abrogation. *Mol Cancer Ther*. 2007;6(4). doi:10.1158/1535-7163.MCT-06-0633

57. Dhar D, Antonucci L, Nakagawa H, et al. Liver Cancer Initiation Requires p53 Inhibition by CD44-Enhanced Growth Factor Signaling. *Cancer Cell*. 2018;33:1061–1077. doi:10.1016/j.ccell.2018.05.003

58. Schlacher K, Christ N, Siaud N, Egashira A, Wu H, Jasin M. Double-strand break repair-independent role for BRCA2 in blocking stalled replication fork degradation by MRE11. *Cell*. 2011;145(4):529-542. doi:10.1016/j.cell.2011.03.041

59. Schlacher K, Wu H, Jasin M. A distinct replication fork protection pathway connects Fanconi anemia tumor suppressors to RAD51-BRCA1/2. *Cancer Cell*. 2012;22(1):106-116. doi:10.1016/j.ccr.2012.05.015

60. Fragkos M, Naim V. Rescue from replication stress during mitosis. *Cell Cycle*. 2017;16(7):613-633. doi:10.1080/15384101.2017.1288322

61. Kitao H, Iimori M, Kataoka Y, et al. DNA replication stress and cancer chemotherapy. *Cancer Sci*. 2017;109:264-271. doi:10.1111/cas.13455

62. Forment J, O'Connor M. Targeting the replication stress response in cancer. *Pharmacol Ther*. 2018;188:155-167. doi:10.1016/j.pharmthera.2018.03.005

63. Bayard Q, Meunier L, Peneau C, et al. Cyclin A2/E1 activation defines a hepatocellularcarcinoma subclass with a rearrangement signatureof replication stress. *Nat Commun*. 2018;9:1-14. doi:10.1038/s41467-018-0755

64. Toledo L, Murga M, Soria R, et al. A cell-based screen identifies ATR inhibitors with synthetic lethal properties for cancer-associated mutations. *Nat Struct Mol Biol*. 2011;18:721-727. doi:10.1038/nsmb.2076

65. Hua X-H, Yan H, Newport J. A Role for Cdk2 Kinase in Negatively Regulating DNA Replication during S Phase of the Cell Cycle. *J Cell Biol*. 1997;137(1):183-192. doi:PMID: 9105046

66. Gnosa S, Capodanno A, Murthy R-V, Jensen L, Sun X-F. AEG-1 knockdown in colon cancer cell lines inhibits radiation-enhanced migration and invasion in vitro and in a novel in vivozebrafish model. *Oncotarget*. 2016;7(49):81634-81644. doi:10.18632/oncotarget.13155

67. Kochanek D, Wells D. CPEB1 regulates the expression of MTDH/AEG-1 and glioblastoma cell migration. *Mol Cancer Res*. 2013;11(2):149-160. doi:10.1158/1541-7786.MCR-12-0498

68. Emdad L, Das S, Dasgupta S, Hu B, Sarkar D, Fisher P. AEG-1/MTDH/LYRIC: Signaling Pathways, Downstream Genes, Interacting Proteins, and Regulation of Tumor Angiogenesis. *Adv Cancer Res*. 2013;120:75-111. doi:10.1016/B978-0-12-401676-7.00003-6

69. Jones R, Mortusewicz O, Afzal I, et al. Increased replication initiation and conflicts with transcription underlie Cyclin E-induced replication stress. *Oncogene*. 2013;32(32):3744-3753. doi:10.1038/onc.2012.387

70. McGrail D, Lin C, Dai H, et al. Defective Replication Stress Response Is InherentlyLinked to the Cancer Stem Cell Phenotype. *Cell Rep*. 2018;23:2095-2106. doi:10.1016/j.celrep.2018.04.068

71. Jeng Y-M, Peng S-Y, Lin C-Y, Hsu H-C. Overexpression and Amplification of Aurora-A in Hepatocellular Carcinoma. *Clin Cancer Res*. 2004;10(6). doi:10.1158/1078-0432.CCR-1057-03

72. Lin Z-Z, Jeng Y-M, Hu F-C, et al. Significance of aurora B overexpression in hepatocellular carcinoma. *BMC Cancer*. 2010;10:461-465. doi:https://doi.org/10.1186/1471-2407-10-461

73. Lin Z-Z, Chou C-H, Cheng A-L, Liu W-L, Cheng J. Radiosensitization by combining an aurora kinase inhibitor with radiotherapy in hepatocellular carcinoma through cell cycle interruption. *Int J Cancer*. 2014;135:492-501. doi:10.1002/ijc.28682

74. Kavanagh B, Lin P, Chen P, Schmidt-Ullrich R. Radiation-induced enhanced proliferation of human squamous cancer cells in vitro: a release from inhibition by epidermal growth factor. *Clin Cancer Res*. 1995;1(12):1557-1562. doi:PMID: 9815956

75. Balaban N, Moni J, Shannon M, Dang L, Murphy E, Goldkorn T. The effect of ionizing radiation on signal transduction: antibodies to EGF receptor sensitize A431 cells to radiation. *Biochim Biophys Acta*. 1996;1314(1-2):147-156. doi:https://doi.org/10.1016/S0167-4889(96)00068-7

76. Goldkorn T, Balaban N, Shannon M, Matsukuma K. EGF receptor phosphorylation is affected by ionizing radiation. *Biochim Biophys Acta*. 1997;1358(3):289-299. doi:https://doi.org/10.1016/S0167-4889(97)00063-3

77. Valerie K, Yacoub A, Hagan M, Curiel D, Fisher P, Dent P. Radiation-induced cell signaling: inside-out and outside-in. *Mol Cancer Ther*. 2007;6(3):789-801. doi:10.1158/1535-7163.MCT-06-0596

VITA

Maheen H. Khan

EDUCATION

Bachelor of Science in Biology — May 2017

Virginia Commonwealth University, Richmond Virginia

Bachelor of Science in Psychology — May 2017

Virginia Commonwealth University, Richmond Virginia

TEACHING EXPERIENCE

Supplemental instruction leader, Department of Biology — August 2016 – May 2017

Virginia Commonwealth University, Richmond, Virginia

Teaching assistant, Honors College — August 2014 – May 2016

Virginia Commonwealth University, Richmond, Virginia

POSTER PRESENTATIONS

Maheen H. Khan, Harshita Nangunuri, and Dr. Joseph Porter: Antidepressant-like effects of the atypical antipsychotic Amisulpride in the differential-reinforcement-of-low-rate (DRL) 72 second operant procedure and in the forced swim task. At the 47th Annual Meeting of the Society for Neuroscience. November 2016.

SERVICE

Reviewed manuscripts submitted to *Scientific Reports*.

Mentoring activities

Anusha Puri (August 2018 – April 2019). High school student. Project: Knockout of AEG-1 Promotes Sensitivity to Human Hepatocellular Carcinoma (HCC). Achievements: VA State Science Fair 2019 2nd place in Biomedical and Health Sciences; Metro Richmond STEM Fair 2019 1st place in Medicine and Health.

ACADEMIC AWARDS & HONORS

Provost Scholarship recipient, Virginia Commonwealth University, August 2013

Business Services Sophomore Year Scholarship recipient, Virginia Commonwealth University, May 2014

Graduation with University Honors, Virginia Commonwealth University, May 2017

Molecular Biology and Genetics M.S. Student Research Support Award recipient, Virginia Commonwealth University, May 2018